Bioconjugate Chemistry

Article

A novel hypoxia-activated anticancer prodrug for bioimaging, tracking drug release, and anticancer application

Wei Liu, Haitong Liu, Xiaoran Peng, Guoqiang Zhou, Dandan Liu, Shenghui Li, Jinchao Zhang, and Shuxiang Wang

Bioconjugate Chem., **Just Accepted Manuscript** • DOI: 10.1021/acs.bioconjchem.8b00511 • Publication Date (Web): 07 Sep 2018

ACS Publications

is published by the American Chemical Society. 1155 Sixteenth Street N.W., Washington, DC 20036

A novel hypoxia-activated anticancer prodrug for bioimaging, tracking drug release, and anticancer application

Wei Liu,[#a] Haitong Liu,[#a] Xiaoran Peng,[a] Guoqiang Zhou,*[a] Dandan Liu,[a] Shenghui Li,[a] Jinchao Zhang,*[a] and Shuxiang Wang*[a]

[a]Key Laboratory of Medicinal Chemistry and Molecular Diagnosis of Ministry of Education, Key Laboratory of Chemical Biology of Hebei Province, College of Chemistry and Environmental Science, Hebei University, Baoding 071002, China

KEYWORDS: hypoxia-activated theranostic prodrug, hypoxic status, oxygen distribution, floxuridine release, two-proton imaging, inhibition tumor growth

ABSTRACT

A novel anticancer theranostic prodrug, FDU-DB-NO_2, specifically activated by hypoxia for selective two-photon imaging hypoxia status, real-time tracking drug release, and solid tumor therapy was designed. The devised prodrug consists of an anticancer drug floxuridine (FDU), a fluorescence dye precursor 4'-(diethylamino)-1,1'-biphenyl-2-carboxylate (DB), and a hypoxic trigger 4-nitrobenzyl group. In normal cells, FDU-DB-NO_2 is "locked". Whereas in tumor cells, the prodrug is "unlocked" by hypoxia and result in fluorescent dye 7-(diethylamino)coumarin (CM) generation along with FDU release. The amounts and rates of CM formation and FDU release were controlled by hypoxic status, and increased with the decreasing of the O_2 concentration. The hypoxic status, distribution of oxygen, and amount of FDU release in tumor cells, spheroids, and tumor tissue could be visualized by fluorescence. FDU-DB-NO_2 showed high cytotoxicity against hypoxic MCF-7 and MCG-803 cell lines, no cytotoxicity against normoxic BRL-3A cells, and exhibited effective inhibition on tumor growth of MCF-7-cell-inoculated xenograft nude mice. This strategy may provide a promising platform for selective two-photon imaging hypoxia status, real-time tracking drug release, and personalized solid tumour treatment.

INTRODUCTION

Chemotherapy remains the main tool for tumor treatment.[1-3] However, traditional chemotherapy always suffers from undesired purgatorial side effects due to their poor selectivity. [4,5] For example, 5-fluorodeoxyuridine (floxuridine, FDU), an analogue of 5-fluorouracil (5-FUra), can be converted to 5-FUra by thymidine phosphorylase and has been widely applied in the therapy in treatment breast, colorectal, and liver cancer.[6] However, its clinical use is limited by severe side effects due to its non-selectivity.[7,8] Therefore, the design chemo-therapeutic agents to selectively kill tumor cells represents a significant challenge for cancer therapy.[9,10] Thus, various efforts have been made to toward the development of prodrugs for controllable active drugs release in tumor tissues that achieve reduced side effects and enhanced therapeutic efficacy. Hypoxia caused by tumor tissues away from the blood vessels is

one important feature of all solid tumors, which leads to a situation that the tumors are not sensitive to chemotherapeutic drugs, and produce drug resistance.[11-14] Hypoxia can also cause an increase reductive stress and lead excess expression of reductases such as nitroreductase (NTR).[15-18] As a result, hypoxia provides a new approach for the diagnostic or treatment of solid tumors. A lot of hypoxia-responsive probes or prodrugs were developed.[19-22] The strategy is an effective tool to design a theranostic agent activated by hypoxia or NTR in hypoxic regions of the individual tumor patient, for timely diagnosis of tumors, and decrease side effects and chemo-resistance.

Theranostic agents possessing both diagnostic and therapeutic capabilities in an all-in-one platform have gained increasing attention due to their low toxicity, decreased side-effects on patients, minimal drug resistance, and improved biodistribution.[23-26] Therefore, theranostic agents research is an emerging and fast-growing field and plays an important role in individual medical.[27-29] Numerous kinds of theranostic agents response to stimuli signals were developed. The stimuli signals may be internal stimuli (such as high acidity,[30-33] high levels of thiols,[34] high levels of reactive oxygen species,[35,36] and specific enzymes over-expression[37,38]) or external stimuli (such as photo irradiation[39]). How to improve the specificity and sensitivity for the targeted cleavage and enhancing therapeutic effect on tumor treatment is becoming the hotspot in cancer treatment.

On the other hand, two-photon fluorescence probes have been extensively applied to investigate a number of biomolecular processes. Comparing to one-photon fluorescence probes, two-photon fluorescence probes possessed some impressive properties (such as deeper penetration depth, less photo-damage to biological specimens, and less photo-bleaching),[40-42] and became a very useful tool for visualization and monitoring biological samples. Coumarin is a two-photon fluorescent dye and has been widely applied to diagnose tumor due to its excellent optical properties related to high molar absorption coefficient and quantum yield.[43-45]

Herein, we designed a promising theranostic prodrug, FDU-DB-NO_2, specifically activated by hypoxia (Scheme 1), using FDU as an active drug, 4-nitrobenzyl group as a hypoxia trigger, and 4'-(diethylamino)-1,1'-biphenyl-2-carboxylate (DB) as a

fluorescence dye precursor. As supposed, FDU-DB-NO_2 is "locked" in normal tissues. Whereas in tumor tissues, bioreductive microenvironment of hypoxia "unlocks" FDU-DB-NO_2 due to the excess expression NTR. Thus, FDU-DB-NO_2 is specifically reduced by NTR with nicotinamide adenine dinucleotide (NADH) under hypoxic conditions and initiates fluorescent dye 7-(diethylamino)coumarin (CM, a coumarin analogue) formation as well as FDU release. In other words, the drug released can be tracked by the signal of fluorescence of CM, which makes it possible to detect the distribution and accumulation of drug in situ and real-time. This strategy provides a promising way to selectively inhibit solid tumor growth, offers a noninvasively way to determine hypoxic status, affords a precise method to analysis of O_2 distribution, and offers an approach to track drug release based on hypoxia status of individual patient.

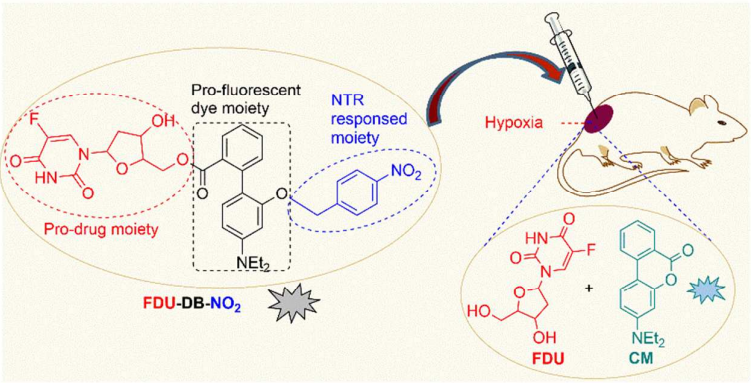

Scheme 1. The structure of FDU-DB-NO_2

RESULTS AND DISCUSSION

Synthesis and characterization. In order to prove the strategy, FDU-DB-NO_2 and fluorescent dye CM were synthesized as shown in Scheme 2. First, 3-methoxyaniline was protected by $(Boc)_2O$ at r.t. to afford *N*-Boc-3-methoxyaniline (**1**). Selective mono-bromination of compound **1** by *N*-bromosuccinimide (NBS) in ethylene glycol dimethyl ether at r.t. afforded *N*-Boc-4-bromo-3-methoxyaniline (**2**). Followed by the deprotection of the *N*-Boc group from compound **2** using HCl (4 mol/L) in anhydrous dioxane at 25 ^{o}C, 4-bromo-3-methoxyaniline (**3**) was generated. Then, 4-bromo-*N,N*-diethyl-3-methoxyaniline (**4**) was prepared *via* ethylation reaction of **3** with bromoethane. Subsequently, the demethylation and nucleophilic substitution

reactions of **4** resulted in the formation of 4-bromo-*N,N*-diethyl-3-(4-nitrobenzyloxy)aniline (**5**). Afterwards, methyl 1,1'-biphenyl-4'-(diethylamino)-2'-(4-nitrobenzyloxy)-2-yl acetate (**6**) was prepared *via* Suzuki cross-couping reaction between **5** with methyl 2-(dihydroxymethyl)benzoate under N_2 atmosphere. Followed by hydrolysis of **6** in sulfuric acid aqueous solution, 1,1'-biphenyl-4'-(diethylamino)-2'-(4-nitrobenzyloxy)-2-carboxylic acid (**7**) was afforded. Finally, in the presence of *N*-diisopropyl carbodiimide (DIC) and dimethyl aminopyridine (DMAP), FDU was conjugated with **7** to generate theranostic prodrug FDU-DB-NO_2. Using similar synthetic method, a control compound (FDU-DB) containing the DB and FDU units without 4-nitrobenzyl group was also synthesized, which was constructed by conjugating of FDU and fluorescent dye precursor. Both of the new compounds and CM were characterized by NMR, IR, and MS (Figure S10-S45, ESI†).

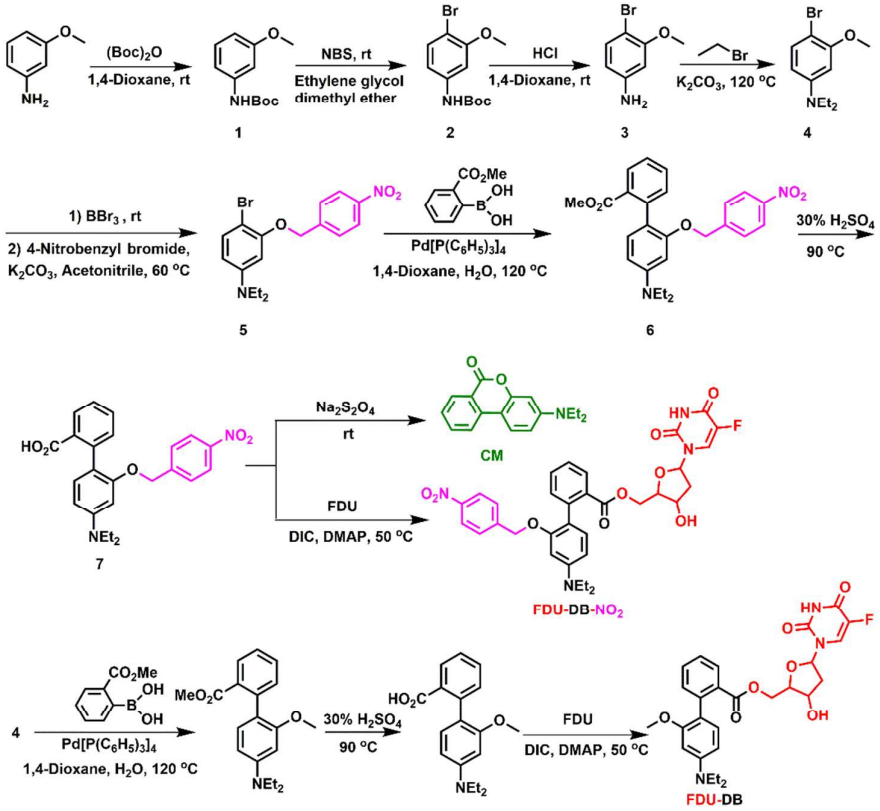

Scheme 2. The synthetic route for FDU-DB-NO_2, FDU-DB, and CM

Mechanism of FDU-DB-NO_2 activated by hypoxia. To demonstrate the mechanism

of FDU-DB-NO_2 activated by hypoxia for generation CM and release FDU, the composition of a reaction mixture of FDU-DB-NO_2 with $Na_2S_2O_4$ [46] was analyzed by HPLC. As shown in Figure S4a~S4c (ESI†), the retention times of FDU, CM, and FDU-DB-NO_2 were 3.081, 21.582, and 26.582 min, respectively. Peaks at 3.091, 21.501 and 26.408 min were observed when the mixture of FDU-DB-NO_2 with $Na_2S_2O_4$ was stirred at 25 °C for 40 mins (Figure S4d, ESI†), they were attributed to anticipated products of FDU, CM, and unreacted FDU-DB-NO_2. This result indicated that FDU-DB-NO_2 is reduced by $Na_2S_2O_4$ and generated CM and FDU simultaneously. Then, the amounts of CM and FDU generated from FDU-DB-NO_2 were also analyzed by HPLC (Figure S5, ESI†). The result showed that the amount of FDU information was nearly equal to that of CM release. Thus, the mechanism of generation CM and release FDU is described as follows (Scheme 3): First, –NO_2 group of FDU-DB- NO_2 is reduced to –NH_2 group by $Na_2S_2O_4$, and FDU-DB-NO_2 is converted to FDU-DB-NH_2. Followed by 1,6-rearrangement-elimination reaction, 4-methylenecyclohexa-2,5-dien-1-imine is removed from FDU-DB-NH_2, and FDU-DB is generated. Finally, through the rotation of the σ bond and a spontaneous intramolecular transesterification reaction, CM was formed as well as FDU was released.

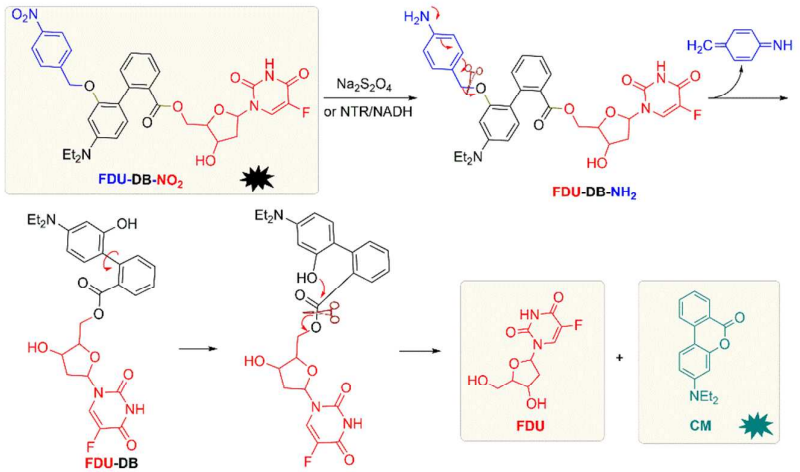

Scheme 3. The mechanism of FDU-DB-NO_2 release CM and FDU under hypoxic conditions

Response of FDU-DB-NO_2 to hypoxia. Next, the amounts and speeds of FDU and CM formation from FDU-DB-NO_2 were investigated. Firstly, the optical properties of

CM and FDU-DB-NO_2 were determined in PBS buffer (0.2 M, contained 0.1% DMSO, pH = 7.4). The absorption spectra of CM and FDU-DB-NO_2 were determined (Figure 1a). As shown in Figure 1b, CM exhibited a strong green fluorescence at 530 nm (λex=380 nm), whereas FDU-DB-NO_2 displayed almost no fluorescence due to the rotation of the $\sigma_{c\text{-}c}$ bond and the quenching effect of 4-nitrobenzyl group. As expected, under N_2 atmosphere at 37 ^{o}C, the mixture of FDU-DB-NO_2 incubation with NTR (in the presence of NADH) displayed a strong green fluorescence at $\lambda_{ex/em}$=380/530 nm (Figure 1c). In addition, the fluorescence intensity increased gradually with the prolongation of reduction time, and the fluorescence intensity reached the highest value when the mixture was incubated about 10 min (Figure 1c and 1d), and it was about 17-fold enhanced compared with that of the mixture was incubated at 0 min. By comparison, the same mixture of NTR, NADH, and FDU-DB-NO_2 in PBS buffer under normoxic conditions (20% O_2) showed very weak fluorescence. The obvious fluorescence enhancement at $\lambda_{ex/em}$=380/530 nm indicated that the 4-nitrobenzyl group of FDU-DB-NO_2 was reduced by NTR/NADH under hypoxic conditions, and a fluorescence dye CM was generated. This, combined with the experimental results of the composition of FDU-DB-NO_2 reduced by $Na_2S_2O_4$ (Figure S4d, ESI†) and the amounts of CM and FDU generated from FDU-DB-NO_2 (Figure S5, ESI†), we were confident that CM and FDU were generated simultaneously, the amount of FDU information was nearly equal to that of CM release, and the fluorescence dye CM could be used as a reporter for in situ and real-time reporting the amount and the distribution of FDU in cancer cells. These results collectively proved that FDU-DB-NO_2 responded to NTR under hypoxic conditions with high sensitivity and quickly speed (about 10 min), CM could be used as a reporter for in situ and real-time reporting the amount and the distribution of FDU release.

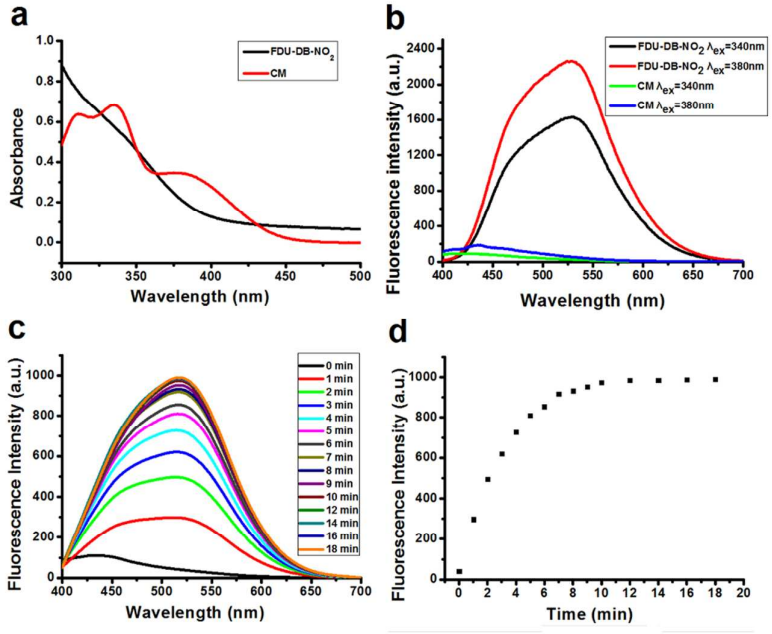

Figure 1. Absorbance (a) and fluorescence (b) of FDU-DB-NO_2 and CM (λ_{ex}=380 nm); Fluorescence intensity of FDU-DB-NO_2 ($\lambda_{ex/em}$=380/530 nm) incubated with NTR (c and d) under hypoxic conditions (1% O_2)

The selectivity and stability of FDU-DB-NO_2. According to above mechanism, we investigated the selectivity of FDU-DB-NO_2 to NTR by determination the changes of fluorescence intensity. As shown in Figure S1 (ESI†), FDU-DB-NO_2 uniquely responded to NTR (in the presence of NADH) under N_2 atmosphere at 37 ^oC and produced a strong enhancement of fluorescence at 530 nm, whereas FDU-DB-NO_2 exhibited nearly no remarkable fluorescence enhancement responses to other reductant (vitamin C), biothreitol (cysteine and glutathione), saccharides (glucose and fructose), and amino acids (glutamic acid, aspartic acid, and histidine) under the same condition. These results showed that FDU-DB-NO_2 possessed remarkable selectivity to NTR under hypoxia conditions.

The stability in biological media is a key parameter of theranostic agents. To investigate the stability of FDU-DB-NO_2, the changes of fluorescence intensity and absorbance of a mixture solution of FDU-DB-NO_2 (100 μM) in blood serum and PBS buffer ($V_{\text{blood serum}}/V_{\text{PBS}}$ =5/1, 37 ^oC) was determined at different time. As shown in Figure S2a and S2b (ESI†), negligible fluorescence intensity and absorbance change of this mixture solution was found. These results demonstrated that theranostic

prodrug FDU-DB-NO_2 exhibited significant stability in blood serum, and the excellent property endowed it with a potential application in biological media.

Furthermore, the effect of pH values on the stability of FDU-DB-NO_2 was evaluated. The fluorescence intensity and absorbance of FDU-DB-NO_2 in PBS buffer at different pH values were tested. As shown in Figure S3a (ESI†), no obvious fluorescence change of FDU-DB-NO_2 in PBS buffer was found in a wide pH range 2 to 10, and no obvious fluorescence change of CM in PBS buffer in the range 4 to 10. In addition, no obvious absorbance change of FDU-DB-NO_2 in PBS buffer was found in the pH range 5-12 (Figure S3b, ESI†). These results showed that FDU-DB-NO_2 possessed excellent stability in PBS buffer at pH 5-10.

All above results suggested that FDU-DB-NO_2 possessed excellent stability under physiological conditions, and showed remarkable selectivity to NTR.

Cellular fluorescence imaging. Subsequently, the effect of the hypoxic status on the amount of CM released from FDU-DB-NO_2 in tumor cells was investigated by laser confocal microscopy. Due to the characteristics of two-photon excitation, CM could be excited by NIR light (λ_{ex}=760 nm) with higher resolution. As shown in Figure 2, MGC-803 cells incubated with FDU-DB-NO_2 under normoxic conditions (20% O_2) showed no fluorescence. However, MGC-803 cells incubated with FDU-DB-NO_2 under hypoxic conditions (1% O_2, 3% O_2, 5% O_2, or 10% O_2) showed noticeable fluorescence, and the fluorescence intensity was increased with the increase of the degree of hypoxia. When the content of oxygen is 1%, a strong green fluorescence was observed, while the oxygen content is 10%, only a weak fluorescence was observed. It indicated that the amount of CM formation was depended on the hypoxic status. A similar result was obtained by one proton emission (λ_{ex}=380 nm, Figure S6, ESI†). And similar results were observed in MCF-7 cells incubated with FDU-DB-NO_2 normoxic and hypoxic conditions (Figure S7 and S8, ESI†). These results illustrated that FDU-DB-NO_2 possessed reliable diagnostic capability for detection of hypoxic status in tumor cells.

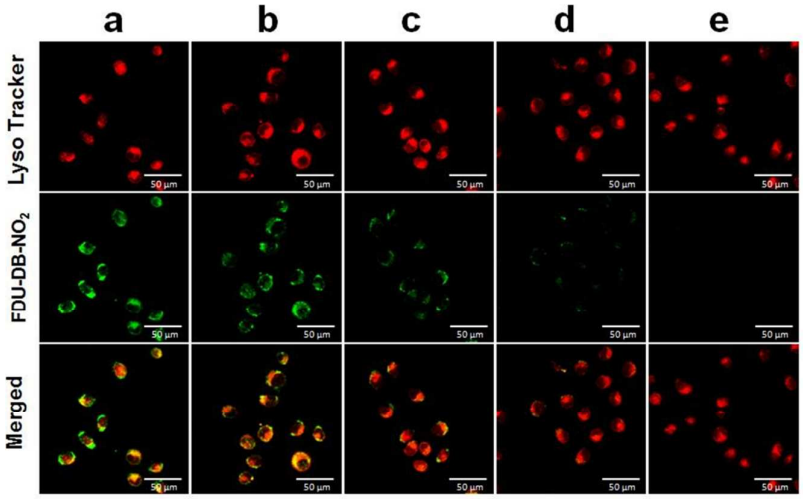

Figure 2. Two-photon confocal fluorescence images of MGC-803 cells incubated with FDU-DB-NO_2 for 12 h under different hypoxic conditions (a: 1% O_2, b: 3% O_2, c: 5% O_2, and d: 10% O_2) and normoxic conditions (e: 20% O_2), lyso-tracker red: λex=577 nm, λem=590 nm

Due to tumor spheres are more closely related to the heterogeneity of the tumor microenvironment with a normoxic surface and a hypoxic core compared with traditional adhere cell cultures.[47] As shown in Figure 3a, MGC-803 and MCF-7 spheres cells incubated with FDU-DB-NO_2 showed strong fluorescence in the core of spheroids and weak fluorescence on the surface of spheroids. Even though the core areas was more acidic than the exterior of spheroids, the strong fluorescence of lyso-tracker red on the surface and very weak fluorescence in the core of spheroids was found due to diffusion of dye molecules. The relative fluorescent intensity distribution from a cross section of tumor spheres (Figure 3b) was consistant with the content of oxygen decreased from surface to core in these tumor spheres. It illustrated that FDU-DB-NO_2 possessed diagnostic capability and sensitivity to monitor the distribution of oxygen in the tumor micro-environment.

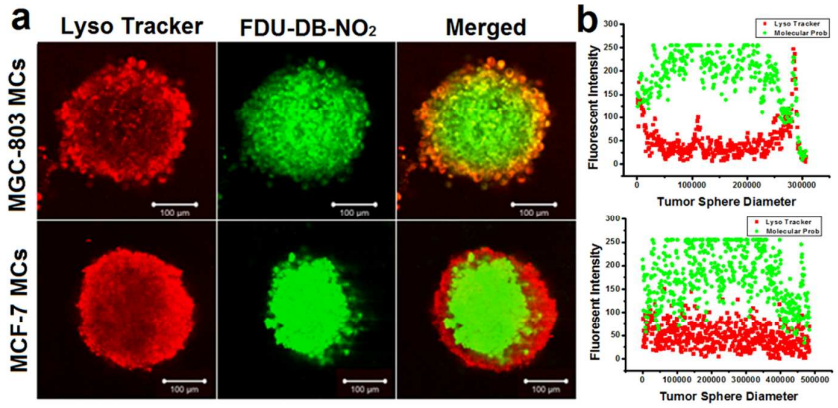

Figure 3. Confocal fluorescence images of MGC-803 and MCF-7 tumor spheres incubated with FDU-DB-NO_2 and lyso-tracker red for 12 h (a); the relative intensity distribution of fluorescence in MGC-803 and MCF-7 tumor spheres (b)

Finally, *in vivo* experiments for examining the selective imaging of tumor tissue of MCF-7-cell-inoculated xenograft nude mice injected with FDU-DB-NO_2 via *in situ* injection were performed. As shown in Figure 4, the beneficial results of the living cell researches led us to further apply FDU-DB-NO_2 to trace hypoxia in the living tumor tissue. For a control experiment (injected with saline), the tumor tissue slides displayed almost no fluorescence (Figure S9, ESI†). In sharp contrast, tumor tissue slides treated with FDU-DB-NO_2 displayed green emission up to a depth of 60 μm. The result demonstrated that FDU-DB-NO_2 can detect basal levels of hypoxia in living tissues.

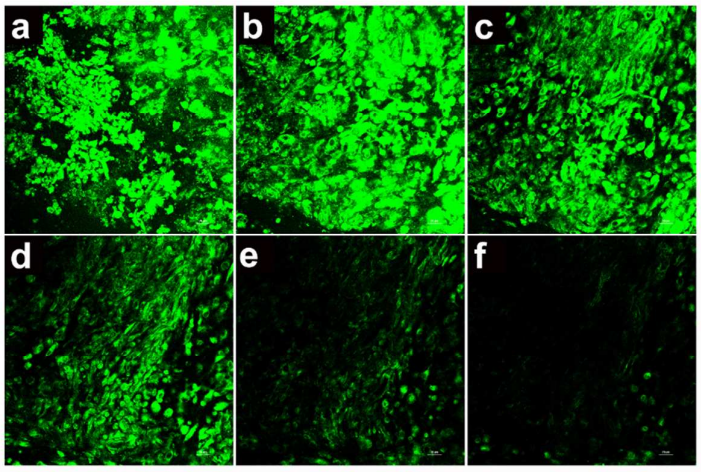

Figure 4. Confocal fluorescence images of tumor tissue treated with FDU-DB-NO_2 (30 μM) for 1 h in different depth of 10 (a), 20 (b), 30 (c), 40 (d), 50 (e), and 60 μm (f)

***In vitro* cytotoxicity of FDU-DB-NO_2.** To investigate the inhibitory effect of FDU-DB-NO_2 on cancer and normal cells, the cell viability of MGC-803, MCF-7, and BRL-3A cells incubated with FDU, FDU-DB-NO_2, or FDU-DB alone was evaluated *via* 3-(4,5-dimethylthiazol-2-yl)-2,5-diphenyltetrazolium bromide (MTT) assay. FDU showed high cytotoxicity against MGC-803 cells line under normoxic (20% O_2) or hypoxic (3% O_2) conditions, and the cell viability of MGC-803 cells was decreased along with the increasing concentration of FDU (Figure 5a and 5b). In addition, FDU-DB-NO_2 exhibited no cytotoxicity against MGC-803 cells under normoxic conditions (20% O_2). However, FDU-DB-NO_2 exhibited high cytotoxicity against MGC-803 cells under hypoxic conditions (3% O_2), and the cell viability of MGC-803 cells decreased with the increase of FDU-DB-NO_2 concentration. Similar results were obtained when MCF-7 cells were incubated with FDU-DB-NO_2 under normoxic (20% O_2) and hypoxic conditions (3% O_2) (Figure 5c and 5d). In view of the complexity of intracellular enzymes (such as hydrolases) in hypoxic tumors, the cell viability of MCF-7 incubated with FDU-DB containing the DB and FDU units without 4-nitrobenzyl group was evaluated. FDU-DB exhibited no cytotoxicity to cells under normoxic (20% O_2) or hypoxic (3% O_2) conditions (Figure 5d). The result indicated that FDU-DB could not be significantly hydrolyzed by hydrolases, and then nitroreductase played a major contribution to cytotoxicity of FDU-DB-NO_2 against hypoxic tumors. As shown in Figure 5e and 5f, incubated with FDU under normoxic conditions (20% O_2), the cell viability of BRL-3A cells decreased along with the increasing concentration of FDU. Meanwhile, the cell viability of BRL-3A cells was almost no obvious change when they were incubated with FDU-DB-NO_2 under normoxic conditions (20% O_2). These results suggested that FDU-DB-NO_2 possessed hypoxia selectivity, exhibited high cytotoxicity against hypoxic cancer cells, and showed non-cytotoxicity against normal cells. Furthermore, flow cytometry studies were used to further verify the cell apoptosis of MGC-803 cells incubated with FDU-DB-NO_2 under hypoxic conditions (3% O_2). As shown in Figure 5, incubation for 12 h, the late apoptotic percentage of MGC-803 cells was only 10.2%, prolonging of incubation time to 24 h, the late apoptotic percentage of MGC-803 cells increases

to 47.3% induced by FDU-DB-NO_2 under hypoxic conditions (3% O_2). All these results demonstrated that FDU-DB-NO_2 showed quite good therapeutic effects on hypoxic cancer cells with non-cytotoxicity to normal cells.

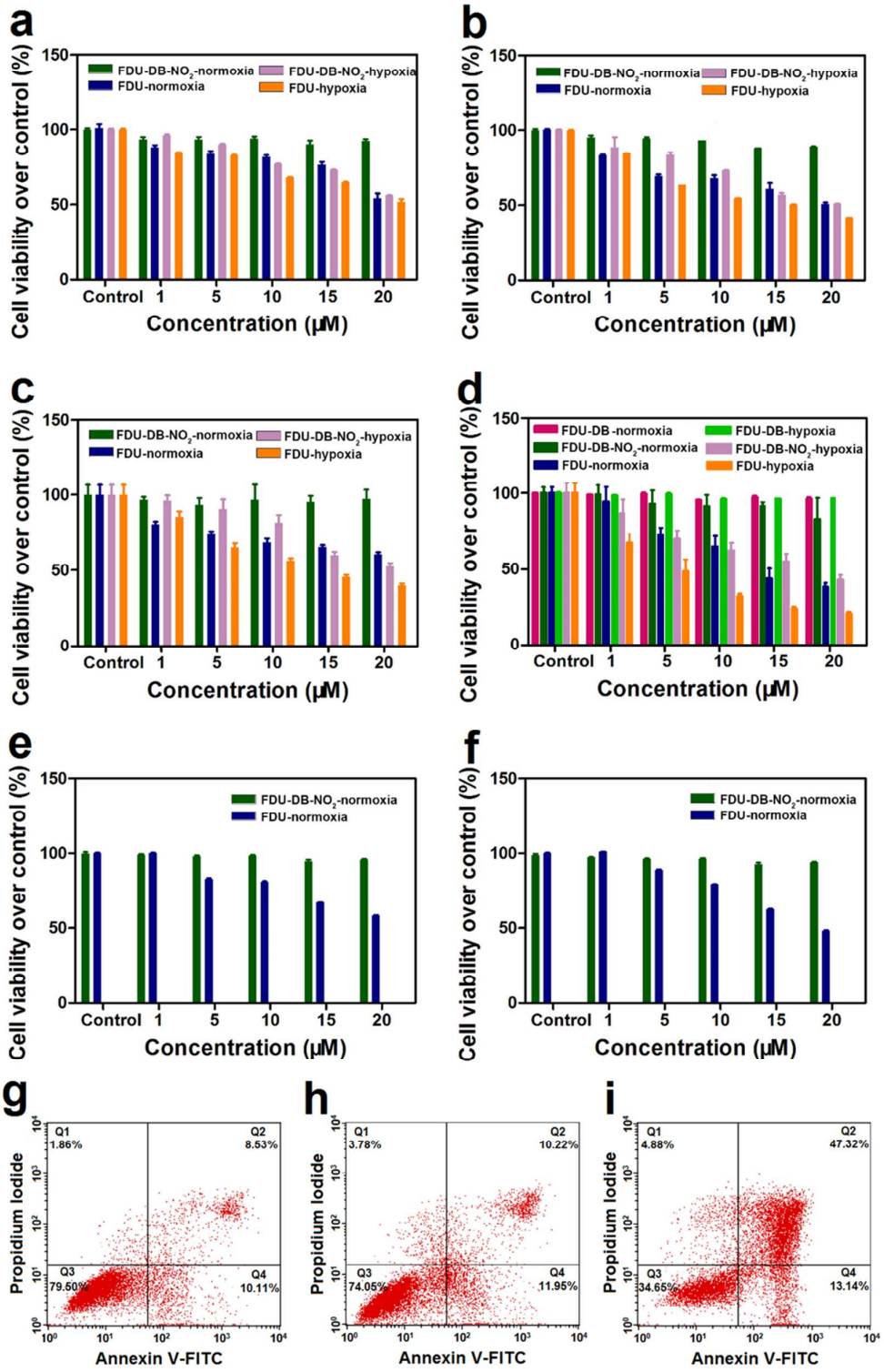

Figure 5. Cell viability of MGC-803 cells (a: 24 h, b: 48 h) incubated with FDU and FDU-DB-NO_2 under normoxic (20% O_2) and hypoxic (3% O_2) conditions; Cell viability of MCF-7 cells (c: 24 h) incubated with FDU and FDU-DB-NO_2 under normoxic (20% O_2) and hypoxic (3% O_2) conditions; Cell viability of MCF-7 cells (d: 48 h) incubated with FDU, FDU-DB-NO_2, and FDU-DB under normoxic (20% O_2) and hypoxic (3% O_2) conditions; cell viability of BRL-3A cells incubated with FDU and FDU-DB-NO_2 under normoxic (20% O_2) conditions (e: 24 h, f: 48 h); apoptosis and necrosis analysis of MGC-803 cells by flow cytometry (g: control, h: incubated with FDU-DB-NO_2 under hypoxic conditions (3% O_2) for 12 h, i: incubated with FDU-DB-NO_2 under hypoxic (3% O_2) conditions for 24 h

In vivo tumor inhibition of FDU-DB-NO_2. Owing to the significant cytotoxicity of FDU-DB-NO_2 against hypoxic cancer cells *in vitro*, the *in vivo* anticancer potential of FDU-DB-NO_2 in MCF-7-cell-inoculated xenograft mice was investigated. The volumes of the xenograft tumours injected with FDU-DB-NO_2 were recorded and compared with the control group (injected with saline). After the *in situ* injection was repeated 4 times (on 0^{th}, 4^{th}, 8^{th}, and 12^{th} day), the tumor tissues were dissected on 14^{th} day. As shown in Figure 6 and Table S1 (ESI†), the tumor growth was markedly inhibited by intratumor injection of FDU-DB-NO_2 compared with the control group which continued to increase in size throughout the processes of the experiments. On the 14^{th} day, the mean volumes of the xenograft tumours injected with FDU-DB-NO_2 was only 63.810 mm^3 with a tumor inhibiting ratio of over 86%, compared with 468.067 mm^3 of the control group. It validated that FDU-DB-NO_2 in hypoxic tumor tissues was selectively activated and released FDU for selective inhibition tumor growth. Meanwhile, a slight body weight increase during this period indicated that no extreme toxicity was associated with these treatments *in vivo*. These results demonstrated that FDU-DB-NO_2 activated by hypoxia was very efficient way for cancer treatment with low side effects due to its hypoxia selectivity. This significant inhibition tumor growth by FDU-DB-NO_2 indicated that the strategy may serve a new promising candidate for potential applications in solid tumor therapy.

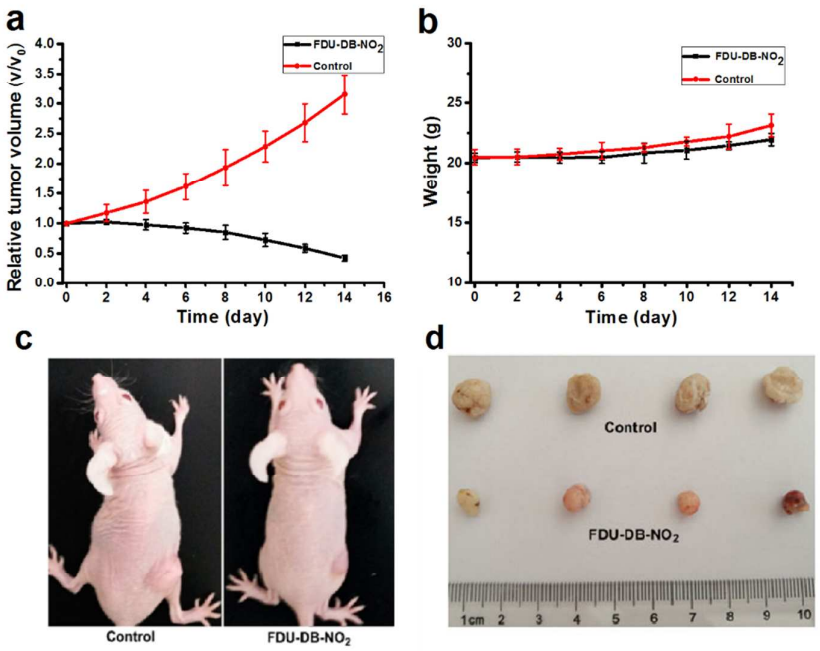

Figure 6. The relative tumor volume (a) and the weight (b) of MCF-7-cell-inoculated xenograft mice treated with FDU-DB-NO_2

CONCLUSION

In summary, we successfully developed an anticancer theranostic prodrug (FDU-DB-NO_2) for diagnosis and therapy solid tumor. FDU-DB-NO_2 was formed by a hypoxia response group, a fluorescent dye precursor, and an anticancer drug. It is in "lock" status in normal cells, whereas it is "unlocked" specifically by hypoxic environment in solid tumor cells, and releases CM and FDU simultaneously. The amounts and rates of CM formation and FDU release were controlled by the hypoxic status, and increased with the decrease of the O_2 concentration. FDU-DB-NO_2 showed high selective identification of hypoxic tumor cells and could be used to detect the hypoxia status, distribution of oxygen, and amount of FDU release in tumor cells, tumor spheres, and tumor tissue. It showed high cytotoxicity against hypoxia tumor cells, and non-cytotoxicity against normal cells, and significent inhibitation tumor growth of MCF-7-inoculated xenograft mice. The strategy will provide a novel and promising platform for construction theranostic prodrugs activated by hypoxia to inhibit tumor growth, non-invasive monitor hypoxia status, distribution of oxygen,

and active drug release, which possesses great potential to be applied in the diagnosis and personalized solid cancer treatment.

EXPERIMENTAL SECTION

Materials. FDU, DMSO, and bovine serum albumin (BSA) were purchased from Alfa-aesar. *m*-Anisidine, 2-methoxycarbonyl phenylboronic acid, NBS and tetrakis(triphenylphosphine)palladium were purchased from Energy Chemical. NTR powder from *Escherichia coli* (≥100 units/mg), and NADH powder were obtained from Sigma-Aldrich. The lyophilized NTR was dissolved in tri-distilled water, which was subsequently divided into 20 parts and stored at −20 °C. The NTR solution was uncongealed before use, and this process did not affect the activity. MTT, benzylpenicillin and streptomycin were obtained from Sigma. Lyso-tracker® red was purchased from Life Technologies. MCF-7, MGC-803, and BRL-3A cells were purchased from Amoresco LLC. All cell (MCF-7, MGC 803, and BRL-3A) lines were purchased from Beijing Union Cell Resource Center (Beijing, China). Four-weeks-old immunodeficient nude mice (BALB/c) were obtained from Beijing Vital River Laboratory Animal Technology Co., Ltd. (Beijing, China).

Instrumentation. The IR spectra were determined with a Thermo Scientific Nicolet iS10 spectrophotometer using KBr pellets. NMR spectra were determined with a Bruker AVANCE III 600 NMR spectrometer (CD_3Cl or DMSO-d_6 as the solvent). Apoptosis was measured on Flow cytometer (BD FACS Calibur, America). MS date were measured on 4000 Q TRAP (SCIEX, USA). Fluorescence indensity were determined with a Hitachi F-7000 spectrophotometer (Tokyo, Japan) in 2.5×10 mm quartz cells. Optical density (OD) was determined with a microplate spectrophotometer (BD FACS Calibur, USA). All chromatography tests were carried out with an HPLC (Agilent 1260, Agilent Techn. Germany). The HPLC system was equipped with a binary LC-20AT pump, an SPD-20A UV-vis detector, as well as an RF-10AXL detector. The analytical column was a Waters Symmetry C^{18} column (4.6 mm × 250 mm, 3.5 μm). Fluorescence imaging experiments were carried out with an LSM 880 confocal microscope (Carl Zeiss AG, Germany).

Synthesis of *tert*-butyl (3-methoxyphenyl)carbamate (1). A mixture of 1.00 g of

3-methoxyaniline (8.26 mmol), 2.70 g of $(Boc)_2O$ (12.40 mmol), and 10 mL of dioxane was stirred at 25 °C for 10 h. After the solvent dioxane was evaporated in vacuo to give a crude product which was purified by column chromatography (V_{EA}/V_{PE} = 1/50) to provide 1.63 g of compound **1** as a white solid in 90% yield. Mp: 56.6-57.6 °C. IR (KBr, cm^{-1}): 3338 (N-H), 3112 (Ar-H), 2977 (C-H) , 1607 (C=C). ^1H NMR ($CDCl_3$, 600 MHz, ppm): δ 7.17 (t, J = 7.8 Hz, 1 H), 7.10 (s, 1 H), 6.84 (d, J = 7.8 Hz, 1 H), 6.59 (d, J = 7.8 Hz, 1 H), 6.46 (s, 1 H), 3.80 (s, 3 H), 1.53 (s, 9 H). ^{13}C NMR ($CDCl_3$, 150 MHz, ppm): δ 160.23, 152.62, 139.65, 129.59, 110.71, 108.81, 104.14, 80.53, 55.27, 28.35. MS (ESI), calcd for $C_{12}H_{17}NNaO_3$, *m/z*: 246.1 $[M+Na]^+$; found 246.1 $[M+Na]^+$.

Synthesis of *tert*-butyl (4-bromo-3-methoxyphenyl)carbamate (2). A mixture of 2.30 g of compound **1** (10.3 mmol), 1.90 g of NBS (10.8 mmol), and 30 mL of ethylene glycol dimethyl ether was stirred at 25 ^oC for 1.5 h. Then, the solvent was evaporated in vacuo to provide a crude product which was purified by column chromatography (V_{EA}/V_{PE}=1/50) to provide 2.77 g compound **2** as a white solid in 89.3% yield. Mp: 123.5-124.5 °C. IR (KBr, cm^{-1}): 3330 (N-H), 3110 (Ar-H), 2979 (C-H), 1600 (C=C). ^1H NMR ($CDCl_3$, 600 MHz, ppm): δ 7.38 (d, J = 8.4 Hz, 1 H), 7.31 (s, 1 H), 6.63 (d, J = 8.4 Hz, 1 H), 6.48 (s, 1 H), 3.90 (s, 3 H), 1.52 (s, 9 H). ^{13}C NMR ($CDCl_3$, 150 MHz, ppm): δ 156.28, 152.45, 139.00, 133.00, 111.31, 104.57, 102.80, 80.91, 56.23, 28.33. MS (ESI), calcd for $C_{12}H_{16}BrNNaO_3$, *m/z*: 324.0 $[M+Na]^+$; found 324.0 $[M+Na]^+$.

Synthesis of 4-bromo-3-methoxyaniline (3). Compound **2** (3.60 g, 11.96 mmol), 15 mL of hydrochloric acid (36%), and 30 mL of 1,4-dioxane were mixed and stirred at 25 ^oC for 2 h. Followed by adding 100 mL of water, the mixture solution was adjusted to pH=8 by Na_2CO_3 aqueous solution. Then, the mixture was extracted thrice with 50 mL of ethyl acetate (EA). The combined organic layer was washed thrice with 50 mL of water, dried over Na_2SO_4 (anhydrous), filtered, and concentrated in vacuo to give 1.94 g of compound **3** as a green solid with a yield of 81%. Mp: 94.1-95.0 °C. IR (KBr, cm^{-1}): 3330 (N-H), 3005 (Ar-H), 2972 (C-H), 1629 (C=C). ^1H NMR ($CDCl_3$, 600 MHz, ppm): δ 7.25 (d, J = 3.6 Hz, 1 H), 6.26 (d, J = 2.4 Hz, 1 H), 6.19 (dd, J =

7.2, 2.4 Hz, 1 H), 3.84 (s, 3 H). ^{13}C NMR ($CDCl_3$, 150 MHz, ppm): δ 156.48, 147.19, 133.44, 108.52, 99.71, 99.51, 56.01. MS (ESI), calcd for C_7H_9BrNO, *m/z*: 202.0 $[M+H]^+$; found 202.0 $[M+H]^+$.

Synthesis of 4-bromo-3-methoxy-*N*,*N*-dimethylaniline (4). Compound **3** (2.4 g, 22.0 mmol), K_2CO_3 (3.0 g, 22.0 mmol), and 20 mL of DMF were mixed and stirred at 120 °C for 9 h. After the mixture was cooled to 25 °C, 100 mL of CH_2Cl_2 was added. The organic phase was washed thrice with 50 mL of water, dried over Na_2SO_4 (anhydrous), and concentrated in vacuo to provide a crude product which was purified by column chromatography (V_{EA}/V_{PE}=1/50) to afford 2.01 g compound **4** as a green oil in 78.2% yield. IR (KBr, cm^{-1}): 3029 (Ar-H), 2970 (C-H), 1594 (C=C).^{1}H NMR ($CDCl_3$, 600 MHz, ppm): δ 7.27 (d, J = 9.0 Hz, 1 H), 6.22 (d, J = 9.0 Hz, 1 H), 6.17 (dd, J = 9.0, 2.4 Hz, 1 H), 3.87 (s, 3 H), 3.33 (q, J = 7.2 Hz, 4 H), 1.16 (q, J = 7.2 Hz, 6 H). ^{13}C NMR ($CDCl_3$, 150 MHz, ppm): δ 156.48, 147.19, 133.44, 108.52, 99.71, 99.51, 56.01. MS (ESI), calcd for $C_{11}H_{17}BrNO$, *m/z*: 257.0 $[M+H]^+$; found 257.8 $[M+H]^+$.

Synthesis of 4-bromo-*N*,*N*-diethyl-3-(4-nitrobenzyloxy)aniline (5). Compound **4** (2.5 g, 10 mmol), 30 mL of DCM, and 6.3 g of borontribromide (25 mmol) were mixed and stirred at -20 °C for 0.5 h. Then, the temperature of the mixture was raised to 25 °C and the reaction was continued for 1.5 h. Next, the reaction mixture was poured into 100 mL of ice water and extracted thrice with 50 mL of DCM. The combined organic phase was washed thrice with 50 mL of water, dried over Na_2SO_4 (anhydrous), and concentrated in vacuo. The obtained residue was dissolved in 15 mL of acetonitrile. Then, 2.2 g of 4-nitrobenzyl bromide (10 mmol) and 2.8 g of K_2CO_3 were added. The mixture was heated to 80 °C and stirred for 3 h. Next, the reaction mixture was concentrated in vacuo, and the residue was purified by flash column chromatography (V_{EA}/V_{PE}=1/30) to afford 2.73 g compound **5** (yellow solid) in 64.2% yield. Mp: 88.9-90.0 °C. IR (KBr, cm^{-1}): 3096 (Ar-H), 2975 (C=C-H), 1593 (C=C), 1562 (-NO_2), 1269 (-C-O-C-). ^{1}H NMR ($CDCl_3$, 600 MHz, ppm): δ 8.26 (d, J = 9.0 Hz, 2 H), 7.69 (d, J = 9.6 Hz, 2 H), 7.31 (d, J = 9.6 Hz, 1 H), 6.23 (d, J = 9.6 Hz, 1 H), 6.18 (s, 1 H), 5.22 (s, 2 H), 3.29 (q, J = 6.6 Hz, 4 H), 1.11 (t, J = 6.6 Hz, 6 H). ^{13}C

NMR ($CDCl_3$, 150 MHz, ppm): δ 155.18, 148.45, 147.57, 144.51, 127.42, 123.81, 106.82, 89.77, 97.25, 69.72, 44.65, 12.42. MS (ESI), calcd for $C_{17}H_{20}BrN_2O_3$, *m/z*: 380.6 $[M+H]^+$; found 380.8 $[M+H]^+$.

Synthesis of methyl 1,1'-biphenyl-4'-diethylamino-2'-(4-nitrobenzyloxy)-2-carboxylate (6). Under N_2 atmosphere, 200 mg of compound **5** (0.53 mmol), 8 mL of DMF, 107 mg of methyl 2-(dihydroxymethyl)benzoate (0.63 mmol), 36.6 mg of tetrakis(triphenylphosphine)palladium (0.032 mmol), 89 mg of Na_2CO_3, and 2 mL of water were stirred and heated to 115 °C for 4 h. After the solution was concentrated in vacuo, the obtained residue was purified by column chromatography (V_{EA}/V_{PE}=1/20) to afford 129 mg of compound **6** (yellow solid) in 56.1% yield. Mp: 93.1-93.9 °C. IR (KBr, cm^{-1}): 3065 (Ar-H), 2925 (C=C-H), 1649 (C=C), 1483 (-NO_2), 1270 (-C-O-C-). ^1H NMR ($CDCl_3$, 600 MHz, ppm): δ 8.12 (d, *J* = 8.4 Hz, 2 H), 7.84 (d, *J* = 7.8 Hz, 1 H), 7.50 (t, *J* = 7.2 Hz, 1 H), 7.38-7.36 (m, 4 H), 7.11 (d, *J* = 8.4 Hz, 1 H), 6.40 (dd, *J* = 8.4, 2.4 Hz, 1 H), 6.17 (d, *J* = 2.4 Hz, 1 H), 5.03 (s, 2 H),3.62 (s, 3 H), 3.33 (q, *J* = 6.6 Hz, 4 H), 1.13 (t, *J* = 6.6 Hz, 6 H). ^{13}C NMR ($CDCl_3$, 150 MHz, ppm): δ 168.83, 155.84, 148.76, 147.24, 145.05, 139.24, 131.65, 131.38, 130.91, 129.46, 126.34, 123.57, 118.59, 105.32, 97.40, 69.58, 51.66, 44.48, 12.65. calcd for $C_{25}H_{27}N_2O_5$, *m/z*: 435.2 $[M+H]^+$; found 434.9 $[M+H]^+$.

Synthesis of 1,1'-biphenyl-4'-diethylamino-2'-(4-nitrobenzyloxy)-2-carboxylic acid (7). Compound **6** (100 mg, 0.23 mmol) and 15 mL of 20% sulfuric acid were stirred and heated to 90 °C for 12 h. After being cooled to about 25 °C, the reaction mixture was adjusted to pH=8 by Na_2CO_3 aqueous solution and extracted thrice with 20 mL of DCM. The combined organic phase was washed thrice with 20 mL of water, dried over Na_2SO_4 (anhydrous), and concentrated in vacuo. The solid residue was purified by column chromatography ($V_{Methanol}/V_{DCM}$= 1/50) to give 57.7 mg of compound **7** (a green solid) in 59.6 % yield. Mp: 199.2-201.6 °C. IR (KBr, cm^{-1}): 3458 (O-H), 3072 (Ar-H), 2965 (C-H), 1682 (C=O), 1522 (-NO_2), 1273 (-C-O-C-). ^1H NMR ($CDCl_3$, 600 MHz, ppm): δ 12.32 (s, 1 H), 8.09 (d, *J* = 9.0 Hz, 2 H), 7.93 (d, *J* = 7.8 Hz, 1 H) , 7.55 (t, *J* = 7.8 Hz, 1 H) , 7.36 (t, *J* = 7.8 Hz, 1 H) , 7.29 (d, *J* = 7.8 Hz, 1 H) , 6.98 (d, *J* = 8.4 Hz, 1 H), 6.30 (d, *J* = 8.4 Hz, 1 H), 6.18 (d, *J* = 2.4 Hz, 1

H), 5.03 (s, 2 H) , 3.33 (q, J = 6.6 Hz, 4 H) , 1.11 (t, J = 6.6 Hz, 6 H).^{13}C NMR ($CDCl_3$, 150 MHz, ppm): δ 173.02, 155.97, 148.99, 147.25, 144.93, 139.36, 131.85, 130.90, 130.43, 130.11, 125.45, 123.59, 105.25, 97.23, 69.54, 44.50, 12.59.calcd for $C_{24}H_{25}N_2O_5$, *m/z*: 421.2 $[M+H]^+$; found 420.9 $[M+H]^+$.

Synthesis of FDU-DB-NO_2. Under N_2 atmosphere, 100 mg of compound **7** (0.24 mmol), 1 mL of DMF, 90 mg of *N,N*-diisopropyl carbodiimide (0.72 mmol), 2.9 mg of 4-dimethylaminopyridine (0.024 mmol), and 58.5 mg of floxuridine (0.24 mmol) were stirred and heated to 50 °C for 18 h. After being cooled to 25 °C, the mixture was purified by column chromatography ($V_{Methanol}/V_{DCM}$=1/50) to provide 9.2 mg of FDU-DB-NO_2 as a green solid. Mp: 90.1-91.4 °C. IR (KBr, cm^{-1}): 3411 (-OH), 3068 (Ar-H), 2966 (C-H), 1718 (C=O), 1682 (C=C), 1556 (-NO_2), 1280 (-C-O-C-), 1074 (C-F). ^{1}H NMR ($CDCl_3$, 600 MHz, ppm): δ 11.78 (s,1 H), 8.12 (d, J = 8.4 Hz, 2 H), 7.73 (d, J = 7.8 Hz, 1 H), 7.62 (d, J = 6.6 Hz, 1 H), 7.58 (t, J = 7.4 Hz, 1 H), 7.47 (d, J = 8.4 Hz, 2 H), 7.38 (t, J = 7.8 Hz, 1 H), 7.34 (d, J = 7.8 Hz, 1 H), 7.00 (d, J = 8.4 Hz, 1 H), 6.32 (d, J = 8.4 Hz, 1 H), 6.21 (s, 1 H), 6.06 (t, J = 6.6 Hz, 1 H), 5.31 (s, 1 H), 5.16 (s, 2 H), 4.18-4.23 (m, 2 H), 3.96 (s, 1 H), 3.79 (q, J = 4.8 Hz, 1 H), 3.32 (q, J = 7.2 Hz,4 H), 1.89-2.01 (m, 2 H), 1.05 (t, J = 7.2 Hz, 6 H). ^{13}C NMR ($CDCl_3$, 150 MHz, ppm): δ 167.74, 156.95, 156.78, 155.44, 148.86, 148.40, 146.62, 145.40, 140.58, 139.05, 138.44, 131.54, 131.40, 131.13, 130.60, 127.47, 124.30, 124.07, 123.24, 104.42, 96.56, 84.38, 83.83, 70.17, 68.32, 62.74, 43.74, 12.59. MS (ESI), calcd for $C_{33}H_{34}FN_4O_9$, *m/z*: 649.2 $[M+H]^+$; found 649.4 $[M+H]^+$.

Synthesis of CM. A mixture of 100 mg of compound **6** (0.23 mmol), 200 mg of $Na_2S_2O_4$ (1.15 mmol), 2 mL of water, and 2 mL of methanol was stirred at 25 °C for 2.5 h. Then 50 mL of water was added and extracted thrice with 50 mL of DCM. The combined organic phase was washed thrice with 50 mL of water, dried over anhydrous Na_2SO_4, and concentrated in vacuo. The solid residue was purified by column chromatography (V_{EA}/V_{PE}=1/30) to give 58.8 mg CM (a green solid) in 92.4% yield. Mp: 85.1-86.6 °C. IR (KBr, cm^{-1}): 3448 (overtone of C=O), 3065 (Ar-H), 2972 (C-H), 1708 (C=O), 1613 (C=C).^{1}H NMR ($CDCl_3$, 600 MHz, ppm): δ 8.30 (d, J = 8.4 Hz, 1 H), 7.90 (d, J = 7.2 Hz, 1 H), 7.81 (d, J = 9.0 Hz, 1 H), 7.70 (t, J = 7.2 Hz, 1 H),

7.37 (t, J = 7.2 Hz, 1 H), 6.65 (d, J = 9.0 Hz, 1 H), 6.56 (s, 1 H), 3.42 (q, J = 7.2 Hz, 4 H), 1.22 (t, J = 7.2 Hz, 6 H). ^{13}C NMR ($CDCl_3$, 150 MHz, ppm): δ 162.18, 153.32, 149.52, 136.17, 134.63, 130.44, 123.73, 120.27, 119.07, 108.81, 106.05, 98.56, 44.68, 12.52. MS (ESI), calcd for $C_{17}H_{18}NO_2$, *m/z*: 268.1 $[M+H]^+$; found 268.2 $[M+H]^+$.

Synthesis of FDU-DB. Under N_2 atmosphere, 100 mg of 4'-(diethylamino)-2'-methoxy-[1,1'-biphenyl]-2-carboxylic acid (0.33 mmol), 1 mL of DMF, 125 mg of *N,N*-diisopropyl carbodiimide (0.99 mmol), 4 mg of 4-dimethylaminopyridine (0.033 mmol), and 98.0 mg of floxuridine (0.40 mmol) were stirred at 50 °C for 18 h. After being cooled to 25 °C, the mixture was purified by column chromatography ($V_{Methanol}/V_{DCM}$=1/50) to provide 30 mg of FDU-DB as a yellow solid. Mp: 189.6-190.8 °C. IR (KBr, cm^{-1}): 3083 (Ar-H), 2969 (C-H), 1716 (C=O), 1613 (C=C), 1273 (-C-O-C-), 1078 (C-F). ^{1}H NMR (DMSO-d_6, 600 MHz, ppm): δ 11.86 (s, 1H), 8,16 (d, J=7.2 Hz, 1H), 7.70 (d, J=7.8 Hz, 1H), 7.56 (t, J=7.2 Hz, 1H), 7.37 (t, J=6.6 Hz, 1H), 7.28 (d, J=7.8 Hz, 1H), 6.98 (d, J=8.4 Hz, 1H), 6.31 (dd, J_1=8.4 Hz, J_2=2.4 Hz, 1H), 6.23 (s, 1H), 5.88 (t, J=6.6 Hz, 1H), 5.30 (t, J=4.8 Hz, 1H), 5.19 (d, J=6.0 Hz, 1H), 3.75 (s, 1H), 3.64 (s, 3H), 3.59 (t, J=4.2 Hz, 2H), 3.38-3.34 (m, 4H), 2.22-2.12 (m, 1H), 2.06 (dd, J_1=13.8 Hz, J_2=5.4 Hz, 1H), 1.09 (t, J=7.2 Hz, 6H), 1.00 (d, J=6.6 Hz, 1H). ^{13}C NMR (DMSO-d_6, 150 MHz, ppm): δ 167.56, 156.58, 148.85, 148.51, 140.73, 139.20, 138.71, 131.48, 131.31, 131.16, 130.23, 128.92, 126.03, 124.48, 124.25, 116.75, 103.87, 94.69, 84.54, 84.43, 75.07, 61.20, 54.72, 43.71, 36.85, 23.25, 12.40. calcd for $C_{27}H_{30}FN_3O_7$, *m/z*: 528.21 $[M+H]^+$; found 528.19 $[M+H]^+$.

Fluorescence intensity of FDU-DB-NO_2 incubated with NTR. DMSO stock solution of FDU-DB-NO_2 (1 mM) was diluted into 100 μM by DMSO and PBS (V_{DMSO}/V_{PBS}= 3/7). Then the solution was incubated with NTR (10 μg/mL) and NADH (2 mM) at 37 ^{o}C under hypoxic condition (1% O_2) for different time (1, 2, 3, 4, 5, 6, 7, 8, 9, 10, 12, 14, 16, and 18 min). Then the fluorescence intensity was detected with a Hitachi F-7000 luminescence spectrophotometer in 2.5×10 mm quartz cells (excited at 380 nm with 2.5/10 nm slit widths, collected from 400 to 700 nm).

Effects of pH value on the stability of FDU-DB-NO_2 and CM. DMSO stock

solution of CM or FDU-DB-NO_2 (1 mM) was diluted to 100 μM by DMSO, and their pH values were adjusted to 2, 3, 4, 5, 6, 7, 8, 9, 10, 11, and 12. Then the fluorescence intensity of the solution was detected with a luminescence spectrophotometer. And the absorbance of the FDU-DB-NO_2 solution was detected with a UV spectrophotometer.

Stability of FDU-DB-NO_2 in blood serum. PBS stock solution of FDU-DB-NO_2 (1 mM) was diluted into 100 μM by a mixture of PBS and blood serum ($V_{PBS}/V_{blood\ serum}$=1/5). The fluorescence intensity and the absorbance of the mixture was detected with the luminescence spectrophotometer and UV spectrophotometer.

Selectivity of FDU-DB-NO_2. DMSO stock solution of FDU-DB-NO_2 (1 mM) were diluted into 100 μM by DMSO and PBS (V_{DMSO}/V_{PBS} = 3/7). Then the solution was incubated with NTR (10 μg/mL) in presence of NADH (2 mM), or cysteine (10 mM), glutathione (10 mM), vitamin C (10 mM), glutamic acid (10 mM), alanine (10 mM), fructose (10 mM), glucose (10 mM), aspartic acid (10 mM), or histidine (10 mM) for 2 h, respectively. The fluorescence intensity of the mixture was detected with a luminescence spectrophotometer.

The HPLC measurement of FDU-DB-NO_2 incubated with $Na_2S_2O_4$. $Na_2S_2O_4$ (10 mg) was added to a solution of FDU-DB-NO_2 (1 μM) in methanol and water ($V_{Methanol}/V_{water}$=1/1), and the mixture was stirred at 25 ^oC for 40 min. Followed by filtration, the filtrate was analyzed by HPLC (Agilent 1260). The HPLC system was performed with a binary LC-20AT pump, an SPD-20A UV-vis detector, as well as an RF-10AXL detector. The analytical column was a Waters Symmetry C^{18} reversed-phase column (4.6 mm ×250 mm, 3.5 μm). The solvent system was composed of two solutions: solution A (water containing 0.05% TFA) and solution B (acetonitrile). The 40 min gradient LC separation include 5 steps: The elution began with a mixture of A and B (*V*/*V*=99/1), followed by a linear increase to 2.5% B over the course of 8.0 min; then 2.5-60% solvent B for 8-15 min (linear); 60-80% solvent B for 15-25 min; then 80% solvent B for 15 min; flow rate of 1.0 mL/min. Detection was carried out with UV light at 254 nm.

The amounts of generated CM and released FDU from FDU-DB-NO_2. Methanol stock solution of FDU (1 mM) and CM (1 mM) were dilute into 25, 50, 75, and 100

μM by methanol and were analyzed by HPLC (Agilent 1260). The standard curves were linear in the range of 25~100 μM. Methanol stock solution of FDU-DB-NO_2 (1 mM) were diluted into 20, 40, 60, 80, and 100 μM by methanol, then these solutions of FDU-DB-NO_2 were incubated with $Na_2S_2O_4$ for 2 h. The amounts of CM generated and FDU released from FDU-DB-NO_2 were analyzed by HPLC.

MTT assay. MCF-7 (or MGC-803 and BRL-3A) cells harvested at subconfluent stage (at a density of 2×10^4 cells/mL) were seeded in 96-well plates and incubated with 200 μL of culture media under the cell culture conditions (5% CO_2, at 37 ^oC) for 12 h. After being incubated with FDU-DB-NO_2 (FDU-DB or FDU) on different concentrations (1, 5, 10, 15, and 20 μM) under normoxic (or hypoxic) conditions for 12 h, and then further incubated for 12 or 36 h. Control wells were carried out by adding culture medium. Banks were prepared by adding culture medium without tumor cells. Subsequently, the cells in 96-well plates were washed twice with PBS buffer, and 10 μL of freshly prepared MTT solution (0.5 mg/mL in PBS buffer) was added into each well and then the cells were incubated for an additional 4 h. Next, 100 μL of DMSO was added into each well at 37 °C for fully dissolve the MTT formazan. The optical density (OD) of formazan solutions was analyzed by a microplate spectrophotometer at 570 nm. The cell viability (%) was presented as $(OD_{sample}-OD_{blank})/(OD_{control}-OD_{blank})\times100$.

Confocal microscopy imaging. MCF-7 (or MGC-803) cells were seeded in confocal dish at a density of 2×10^4 cells/mL under the cell culture conditions (5% CO_2, at 37 ^oC) in a humidified incubator (SANYO, MCO-20AIC, JPN). Then, the medium was replaced with 10 μM FDU-DB-NO_2 in fresh culture medium. After incubation with FDU-DB-NO_2 under normoxic conditions (20% O_2, 5% CO_2, and 75% N_2, at 37 ^oC) or different hypoxic conditions (1% O_2, 5% CO_2, and 94% N_2, at 37 ^oC; 3% O_2, 5% CO_2, and 92% N_2, at 37 ^oC; 5% O_2, 5% CO_2, and 90% N_2, at 37 ^oC; 10% O_2, 5% CO_2, and 85% N_2, at 37 ^oC) in a humidified incubator (Heal Force, HF 100, CHN) for 12 h. Then, the medium was removed and the cells were washed twice with PBS buffer. The fluorescence imaging experiments were carried out on an LSM880 confocal laser scanning microscope (Carl Zeiss AG, Germany) and excited with 380 nm laser light

for one-photon imaging and 760 nm for two-photon imaging.

The cultivation of MGC 803 and MCF-7 spheres. MGC 803 (or MCF-7) cells were diluted in serum free growth medium (1000 cells/mL) and plated in 100 μL in non-tissue culture coated 96-well plates. Cells were fed with 25 μL of serum-free growth medium every other day, for 14 d. The culture medium consisted of serum-free DMEM/F12 supplemented with 10 U/mL heparin, 20 U/mL B27, and 20 U/mL human recombinant fibroblast growth factor. After 14 d, spheres were counted as a tumor sphere forming unit.

Animal experiment. Animal experiments were followed to the guidelines of the Animal Welfare and Ethical Committee of Hebei University. Four weeks old Balb/c nude mice (female, around 20 g) were fed in an animal facility (20±2 °C, 60±10% relative humidity, 12 h light/dark cycle) with free feeding food and drinking water. Tumor-bearing mice models were established by subcutaneous injection of MCF-7 cells (1×10^7 cells each mouse). After the tumors grew to be about 50-80 mm^3, MCF-7-cell-inoculated xenograft mice were divided into two groups (n=5). The first group of mice was treated with FDU-DB-NO_2 *via* in situ injection (on the 0^{th}, 4^{th}, 8^{th}, 10^{th}, and 12^{th} day; 10 mg/kg body weight). The second group was injected with saline (on the 0^{th}, 4^{th}, 8^{th}, 10^{th}, and 12^{th} day) as the control. On the 14^{th} day, mice were killed by CO_2, the tumor tissues were dissected. The body weight and tumor volume of mice were measured every two days, and the tumor volume of mice was calculated as (Tumor length) × $(\text{Tumor width})^2/2$.

MCF-7-cell-inoculated xenograft mice were killed by cervical vertebra dislocation when the tumor grew to the right size. After washing off the blood with PBS, the tumor tissues were cut into about 600 μm thick sections. The tumor tissue slices were incubated with FDU-DB-NO_2 (30 μM) for 1 h. After washing thrice with PBS buffer, the tumor tissue slices were monitored with an LSM 880 confocal microscope excited at 760 nm (TP mode), and the emission wavelengths were collected from 500 nm to 550 nm.

ASSOCIATED CONTENTS

Supporting Information

The supporting Information is available free of charge on the ACS publications websites.

AUTHOR INFORMATION

Corresponding Author

*Guoqiang Zhou, E-mail: zhougq1982@163.com

*Jinchao Zhang, E-mail: jczhang6970@163.com

*Shuxiang Wang, E-mail: wsx@hbu.edu.cn

Author Contributions

#These authors contributed equally to the manuscript

Notes

The authors declare no competing financial interests.

ACKNOWLEDGEMENTS

This work was supported by the Natural Science Foundation of China (21471044, 31500812), the Key Basic Research Special Foundation of Science Technology Ministry of Hebei Province (15962602D), and the Natural Science Foundation of Hebei Province (B2015201213, B2016201169, B2017201226, B2017201230, B2017201135).

REFERENCES

(1) M. Bio, P. Rajaputra, G. Nkepang, Y. You. (2014) Far-red light activatable, multifunctional prodrug for fluorescence optical imaging and combinational treatment. *J. Med. Chem 57*, 3401-3409.

(2) L. K. Penny, H. M. Wallace. (2015) The challenges for cancer chemoprevention. *Chem. Soc. Rev. 44*, 8836-8847.

(3) B. Li, P. Liu, D. Yan, F. Zeng, S. Wu. (2017) A self-immolative and DT-diaphorase-activatable prodrug for drug-release tracking and therapy. *J. Mater. Chem. B 5*, 2635-2643.

(4) Y. Wang, P. Huang, M. Hu, W. Huang, X. Zhu, D. Yan. (2016) Self-delivery nanoparticles of amphiphilic methotrexate-gemcitabine prodrug for synergistic combination chemotherapy via effect of deoxyribonucleotide pools. *Bioconjugate Chem. 27*, 2722-2733.

(5) C. Dong, Z. Liu, S. Wang, B. Zheng, W. Guo, W. Yang, X. Gong, X. Wu, H. Wang, J. Chang. (2016) A protein–polymer bioconjugate-coated upconversion nanosystem for simultaneous tumor cell imaging, photodynamic therapy, and chemotherapy. *ACS Appl. Mater. Inter. 8*, 32688-32698.

(6) M. Hu, P. Huang, Y. Wang, Y. Su, L. Zhou, X. Zhu, D. Yan. (2015) Synergistic combination chemotherapy of camptothecin and floxuridine through self-assembly of amphiphilic drug-drug conjugate. *Bioconjugate Chem. 26*, 2497-2506.

(7) J. L. Grem. (2000) 5-Fluorouracil: Forty-Plus and Still Ticking. A Review of its preclinical and clinical development, Invest. *New Drugs. 18*, 299-313.

(8) H. Nakagawa, N. Maeda, T. Tsuzuki, T. Suzuki, A. Hirayama, E. Miyahara, K. Wada. (2001) Intracavitary chemotherapy with 5-Fluoro-2'-deoxyuridine (FdUrd) in malignant brain tumors. *Jpn. J. Clin. Oncol. 31*, 251-258.

(9) I. Kim, X. Song, B. S. Vig, S. Mittal, H.C. Shin, P. J. Lorenzi, G. L. Amidon. (2004) A novel nucleoside prodrug-activating enzyme: substrate specificity of biphenyl hydrolase-like protein. *Mol. Pharm. 1*, 117-127.

(10) T. Zhang, P. Huang, L. Shi, Y. Su, L. Zhou, X. Zhu, D. Yan. (2015) Self-assembled nanoparticles of amphiphilic twin drug from Floxuridine and Bendamustine for cancer therapy. *Mol. Pharm. 12*, 2328-2336.

(11) K. Xu, F. Wang, X. Pan, R. Liu, J. Ma, F. Kong, B. Tang. (2013) High selectivity imaging of nitroreductase using a near-infrared fluorescence probe in hypoxic tumor. *Chem. Commun. 49*, 2554-2556.

(12) W. Feng, Y. Wang, S. Chen, C. Wang, S. Wang, S. Li, H. Li, G. Zhou, J. Zhang. (2016) 4-Nitroimidazole-3-hydroxyflavone conjugate as a fluorescent probe for hypoxic cells Short communication. *Dyes Pigments 131*, 145-153.

(13) C. C. Huang, W. T. Chia, M. F. Chung, K. J. Lin, C. W. Hsiao, C. Jin, W. H. Lim, C. C. Chen, H. W. Sung. (2016) An implantable depot that can generate oxygen in situ for overcoming hypoxia-induced resistance to anticancer drugs in chemotherapy. *J. Am. Chem. Soc. 138*, 5222-5225.

(14) Z. Xu, J. Zhao, S. Gou, G. Xu. (2017) Novel hypoxia-targeting Pt(IV) prodrugs, *Chem. Commun. 53*, 3749-3752.

(15) H. Shi, R. T. K. Kwok, J. Liu, B. Xing, B. Z. Tang, B. Liu. (2012) Real-time monitoring of cell apoptosis and drug screening using fluorescent light-up probe with aggregation-induced emission characteristics. *J. Am. Chem. Soc. 134*, 17972-17981.

(16) D. Kim, H. Moon, S. H. Baik, S. Singha, Y. W. Jun, T. Wang, K. H. Kim, B. S. Park, J. Jung, I. Mook-Jung, K. H. Ahn. (2015) Two-photon absorbing dyes with minimal autofluorescence in tissue imaging: application to in vivo imaging of amyloid-β plaques with a negligible background signal. *J. Am. Chem. Soc. 137*, 6781-6789.

(17) H. Li, W. Peng, W. Feng, Y. Wang, G. Chen, S. Wang, S. Li, H. Li, K. Wang, J. Zhang. (2016) A novel dual-emission fluorescent probe for the simultaneous detection of H_2S and GSH. *Chem. Commun. 52*, 4628-4631.

(18) H. Li, W. Lei, J. Wu, S. Li, G. Zhou, D. Liu, X. Yang, S. Wang, Z. Li, J. Zhang. (2018) An upconverting nanotheranostic agent activated by hypoxia combined with NIR irradiation for selective hypoxia imaging and tumour therapy. *J. Mater. Chem. B 6*, 2747-2757.

(19) K. Okuda, Y. Okabe, T. Kadonosono, T. Ueno, B. G. M. Youssif, S. Kizaka-Kondoh, H Nagasawa. (2012) 2-Nitroimidazole-tricarbocyanine conjugate as a near-infrared fluorescent probe for in vivo imaging of tumor hypoxia. *Bioconjugate Chem.* 23, 324-329.

(20) J. Liu, Y. Liu, W. Bu, J. Bu, Y. Sun, J. Du, J. Shi. (2014) Ultrasensitive nanosensors based on upconversion nanoparticles for selective hypoxia imaging in vivo upon near-infrared excitation. *J. Am. Chem. Soc. 136*, 9701-9709.

(21) J. Liu, W. Bu, J. Shi. (2017) Chemical design and synthesis of functionalized probes for imaging and treating tumor hypoxia. *Chem. Rev. 117*, 6160-6224.

(22) Y. Ti, L. Yu, Y. Tang, T. Jin, M. Yang, R. Wang, Y. Xu, W. Zhu. (2018) A hypoxia-activated near infrared fluorescent probe for cyclooxygenase-2 and in vivo imaging for tumor and inflammation. *Sens Actuators B Chem. 265*, 582-590.

(23) R. Kumar, J. Han, H. J. Lim, W. X. Ren, J.Y. Lim, J. H. Kim, J. S. Kim. (2014) Mitochondrial induced and self-monitored intrinsic apoptosis by antitumor theranostic prodrug: in vivo imaging and precise cancer treatment. *J. Am. Chem. Soc. 136*,

17836-17843.

(24) M. H. Lee, E.J. Kim, H. Lee, H. M. Kim, M. J. Chang, S. Y. Park, K. S. Hong, J. S. Kim, J. L. Sessler. (2016) Liposomal texaphyrin theranostics for metastatic liver cancer. *J. Am. Chem. Soc. 138*, 16380-16387.

(25) Y. Yuan, B. Liu. (2017) Visualization of drug delivery processes using AIEgens. *Chem. Sci. 8*, 2537-2546.

(26) L. Chambre, A. Degirmenci, R. Sanyal, A. Sanyal. (2018) Multi-functional nanogels as theranostic platforms: exploiting reversible and nonreversible linkages for targeting, Imaging, and drug delivery. *Bioconjugate Chem.* 29, 1885-1896.

(27) W. Feng, C. Gao, W. Liu, H. Ren, C. Wang, K. Ge, S. Li, G. Zhou, H. Li, S. Wang, G. Jia, Z. Li, J. Zhang. (2016) A novel anticancer theranostic pro-prodrug based on hypoxia and photo sequential control. *Chem. Commun. 52*, 9434-9437.

(28) W. S. Shin, M.G. Lee, P. Verwilst, J. H. Lee, S.G. Chi, J. S. Kim. (2016) Mitochondria-targeted aggregation induced emission theranostics: crucial importance of in situ activation. *Chem. Sci. 7*, 6050-6059.

(29) C. Chen, Z. Song, X. Zheng, Z. He, B. Liu, X. Huang, D. Kong, D. Ding, B. Z. Tang. (2017) AIEgen-based theranostic system: targeted imaging of cancer cells and adjuvant amplification of antitumor efficacy of paclitaxel. *Chem. Sci. 8*, 2191-2198.

(30) S. Y. Li, L.H. Liu, H.Z. Jia, W. X. Qiu, L. Rong, H. Cheng, X. Z. Zhang. (2014) A pH-responsive prodrug for real-time drug release monitoring and targeted cancer therapy. *Chem. Commun. 50*, 11852-11855.

(31) L. Fu, C. Sun, L. Yan. (2015) Galactose targeted pH-responsive copolymer conjugated with near infrared fluorescence probe for imaging of intelligent drug delivery. *ACS Appl. Mater. Inter. 7*, 2104-2115.

(32) S. Park, E. Kim, W. Y. Kim, C. Kang, J. S. Kim. (2015) Biotin-guided anticancer drug delivery with acidity-triggered drug release. *Chem. Commun. 51*, 9343-9345.

(33) X. Xue, S. Jin, C. Zhang, K. Yang, S. Huo, F. Chen, G. Zou, X. J. Liang. (2015) Probe-inspired nano-prodrug with dual-color fluorogenic property reveals spatiotemporal drug release in living cells. *ACS Nano 9*, 2729-2739.

(34) M. H. Lee, J. L. Sessler, J. S. Kim. (2015) Disulfide-based multifunctional

conjugates for targeted theranostic drug delivery. *Acc. Chem. Res. 48*, 2935-2946.

(35) E. J. Kim, S. Bhuniya, H. Lee, H. M. Kim, C. Cheong, S. Maiti, K. S. Hong, J. S. Kim. (2014) An activatable prodrug for the treatment of metastatic tumors. *J. Am. Chem. Soc. 136*, 13888-13894.

(36) R. Kumar, J. Han, H. J. Lim, W. X. Ren, J.Y. Lim, J. H. Kim, J. S. Kim. (2014) Mitochondrial induced and self-monitored intrinsic apoptosis by antitumor theranostic prodrug: in vivo imaging and precise cancer treatment. *J. Am. Chem. Soc. 136*, 17836-17843.

(37) P. Liu, J. Xu, D. Yan, P. Zhang, F. Zeng, B. Li, S. Wu. (2015) A DT-diaphorase responsive theranostic prodrug for diagnosis, drug release monitoring and therapy. *Chem. Commun. 51*, 9567-9570.

(38) X. Tian, K. H. Baek and I. Shin. (2013) Dual-targeting delivery system for selective cancer cell death and imaging. *Chem. Sci. 4*, 947-956.

(39) P. Rai, S. Mallidi, X. Zheng, R. Rahmanzadeh, Y. Mir, S. Elrington, A. Khurshid, T. Hasan. (2010) Development and applications of photo-triggered theranostic agents. *Adv. Drug Del. Rev. 62*, 1094-1124.

(40) K. Mutoh, Y. Kobayashi, T. Yamane, T. Ikezawa, J. Abe. (2017) Rate-tunable stepwise two-photon-gated photoresponsive systems employing a synergetic interaction between transient biradical units. *J. Am. Chem. Soc. 139*, 4452-4461.

(41) Z. Mao, H. Jiang, Z. Li, C. Zhong, W. Zhang, Z. Liu. (2017) An N-nitrosation reactivity-based two-photon fluorescent probe for the specific in situ detection of nitric oxide. *Chem. Sci. 8*, 4533-4538.

(42) Y. Li, X. Xie, X. e. Yang, M. Li, X. Jiao, Y. Sun, X. Wang, B. Tang. (2017) Two-photon fluorescent probe for revealing drug-induced hepatotoxicity via mapping fluctuation of peroxynitrite. *Chem. Sci. 8*, 4006-4011.

(43) P. D. McFadden, K. Frederick, L. A. Argüello, Y. Zhang, P. Vandiver, N. Odegaard, D. A. Loy. (2017) UV fluorescent epoxy adhesives from noncovalent and covalent incorporation of coumarin dyes. *ACS Appl. Mater. Inter. 9*, 10061-10068.

(44) X. Xie, F. Tang, X. Shangguan, S. Che, J. Niu, Y. Xiao, X. Wang, B. Tang. (2017) Two-photon imaging of formaldehyde in live cells and animals utilizing a

lysosome-targetable and acidic pH-activatable fluorescent probe. *Chem. Commun. 53* 6520-6523.

(45) K. Iliopoulos, O. Krupka, D. Gindre, M. Sallé. (2010) Reversible two-photon optical data storage in coumarin-based copolymers. *J. Am. Chem. Soc. 132*, 14343-14345.

(46) M. R. Webster, M. Zhao, M. A. Rudek, C. L. Hann, C. L. Freel Meyers. (2011) Bisphosphonamidate clodronate prodrug exhibits potent anticancer activity in non-small-cell lung cancer cells. *J. Med. Chem. 54*, 6647-6656.

(47) X. Zheng, X. Wang, H. Mao, W. Wu, B. Liu, X. Jiang. (2015) Hypoxia-specific ultrasensitive detection of tumours and cancer cells in vivo. *Nat. Commun. 6*, 5834.

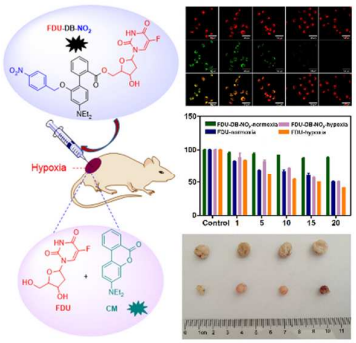

Graphical Abstract

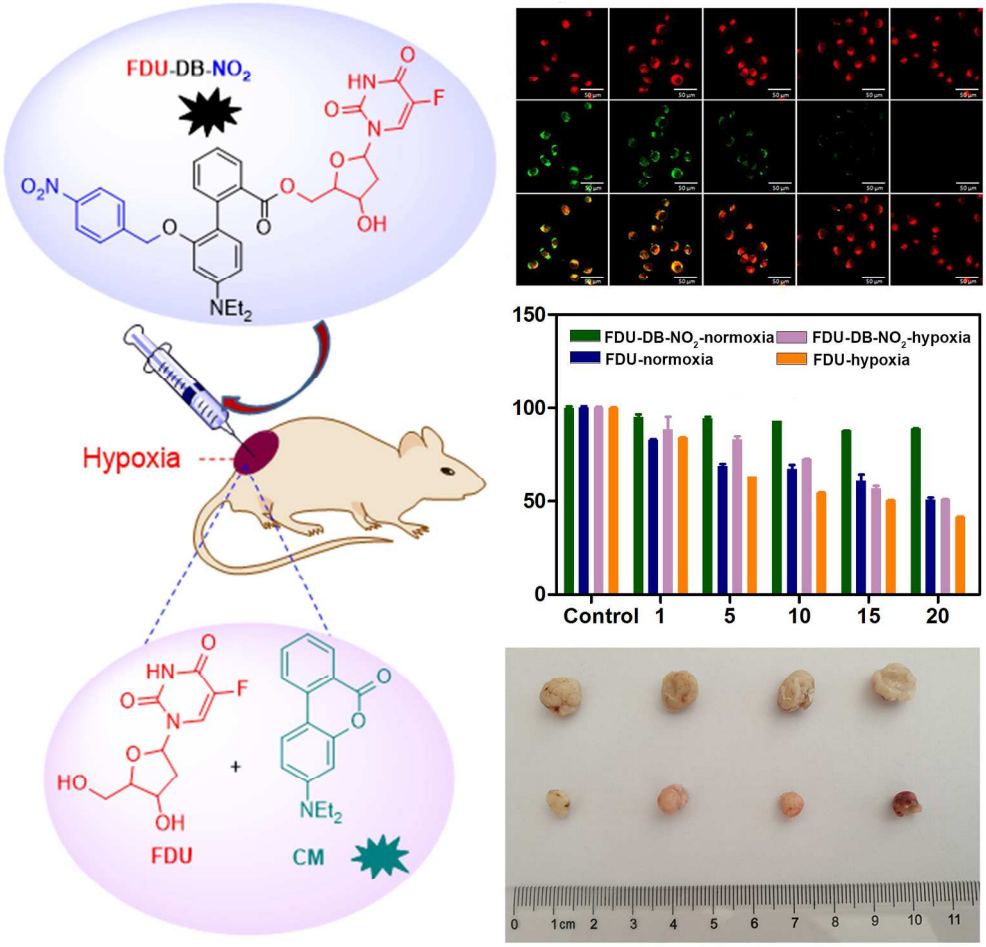

table of content

250x250mm (299 x 299 DPI)

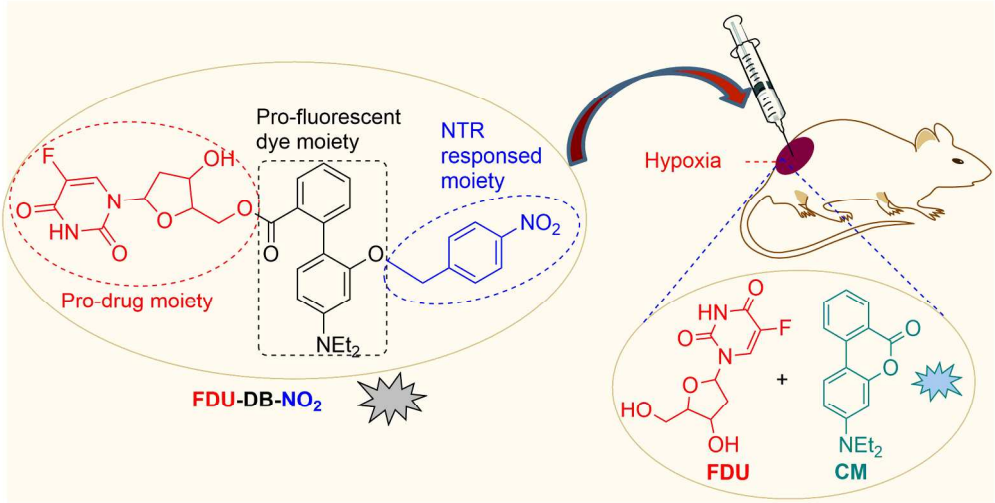

Scheme 1

198x101mm (300 x 300 DPI)

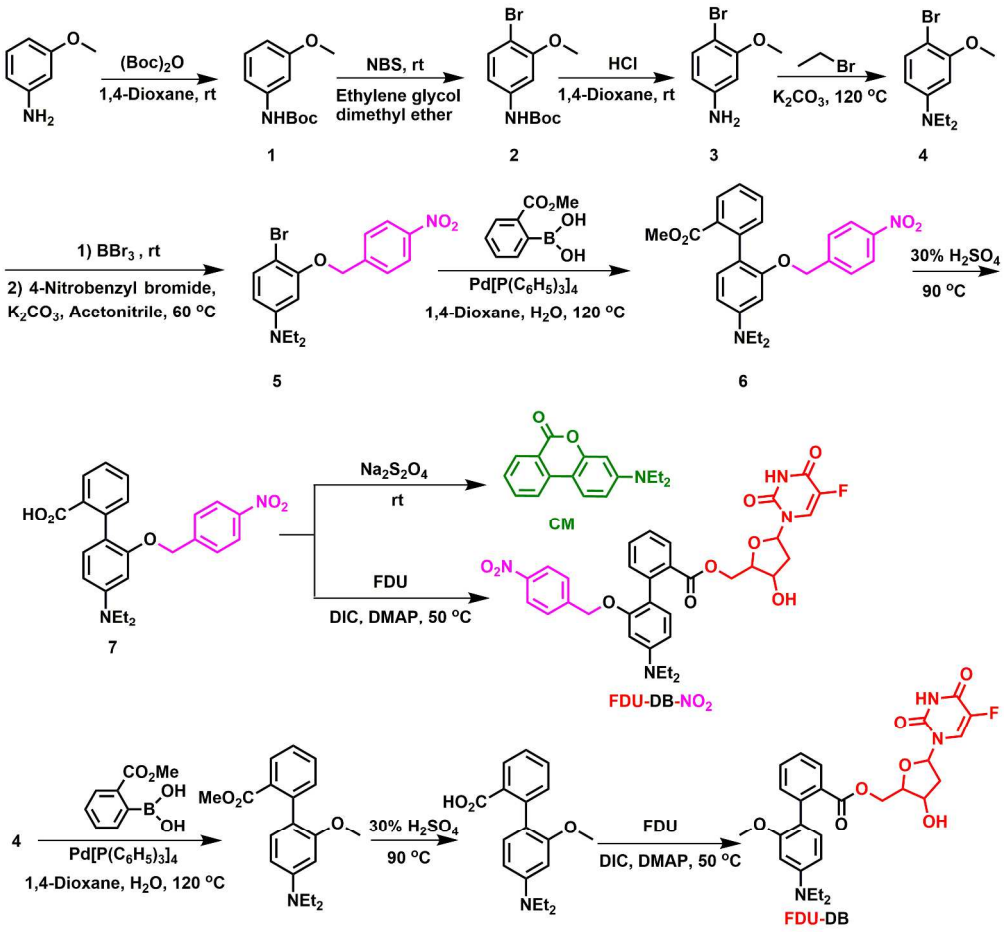

Scheme 2

248x230mm (300 x 300 DPI)

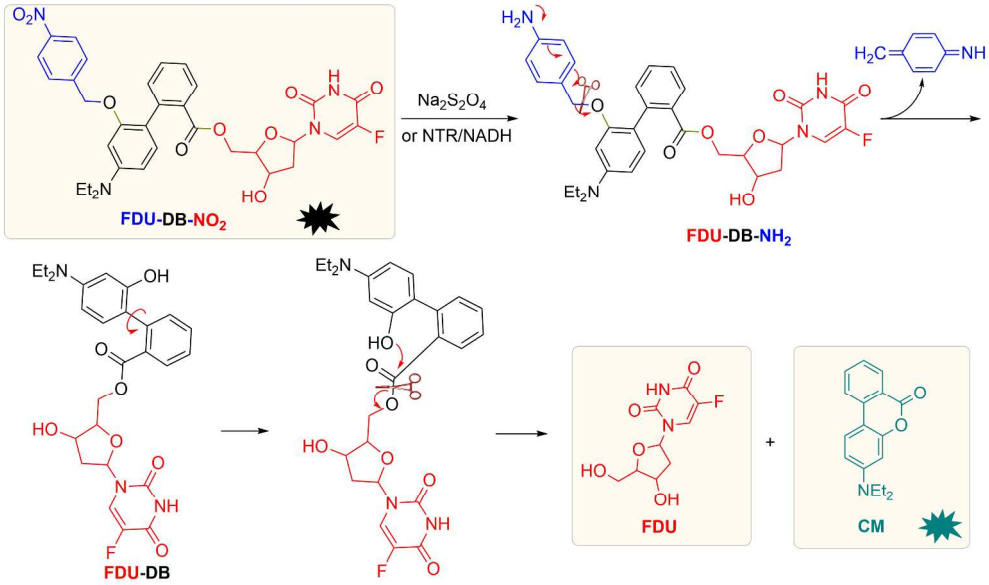

Scheme 3

243x146mm (300 x 300 DPI)

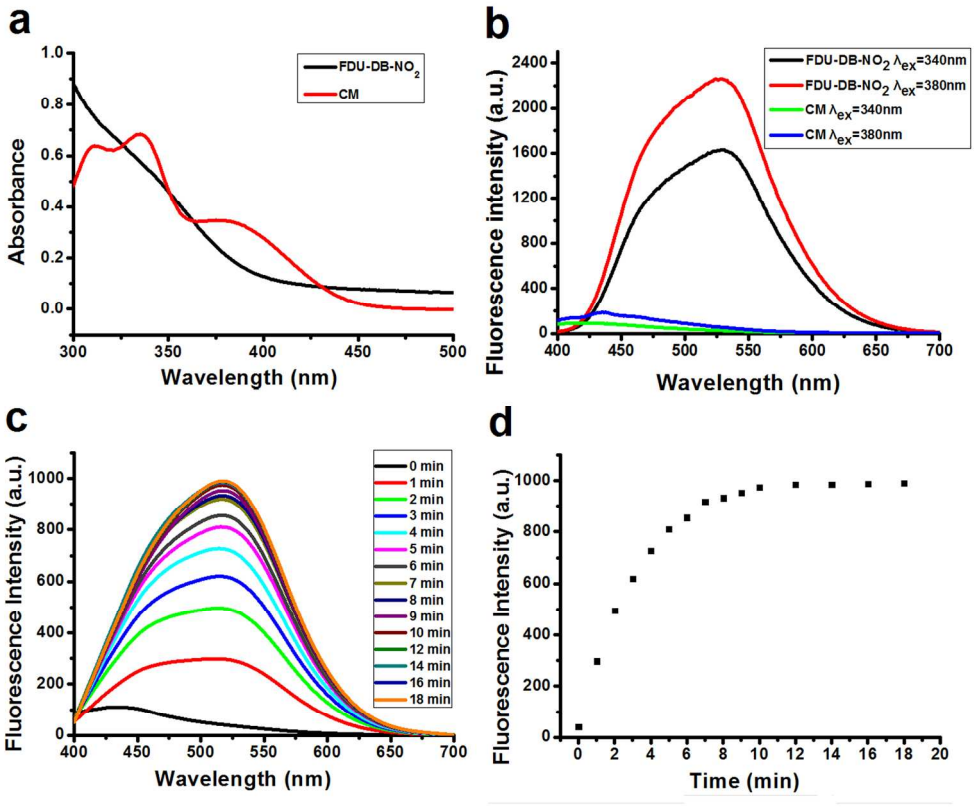

Figure 1

171x140mm (300 x 300 DPI)

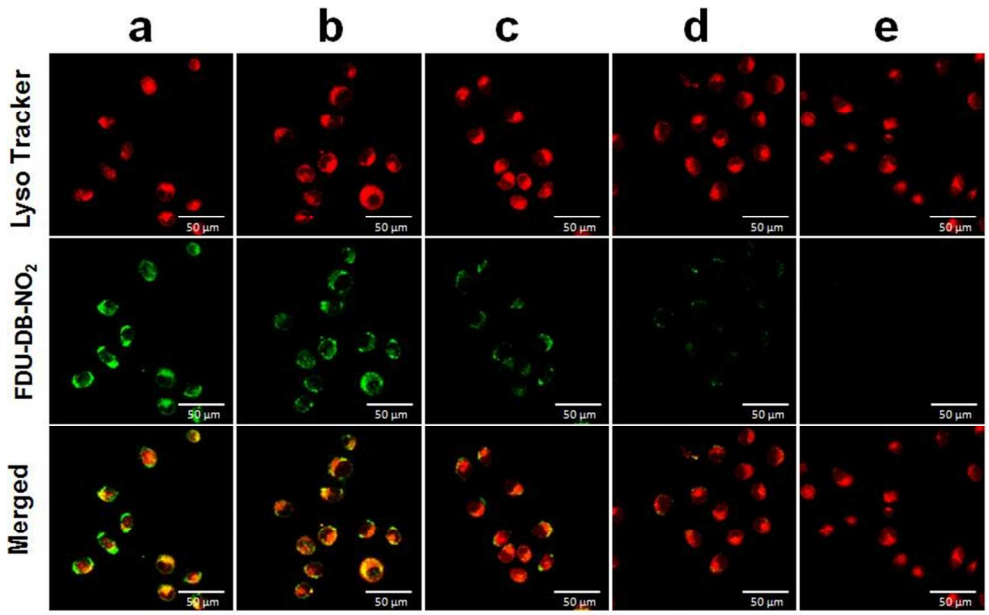

Figure 2

231x145mm (300 x 300 DPI)

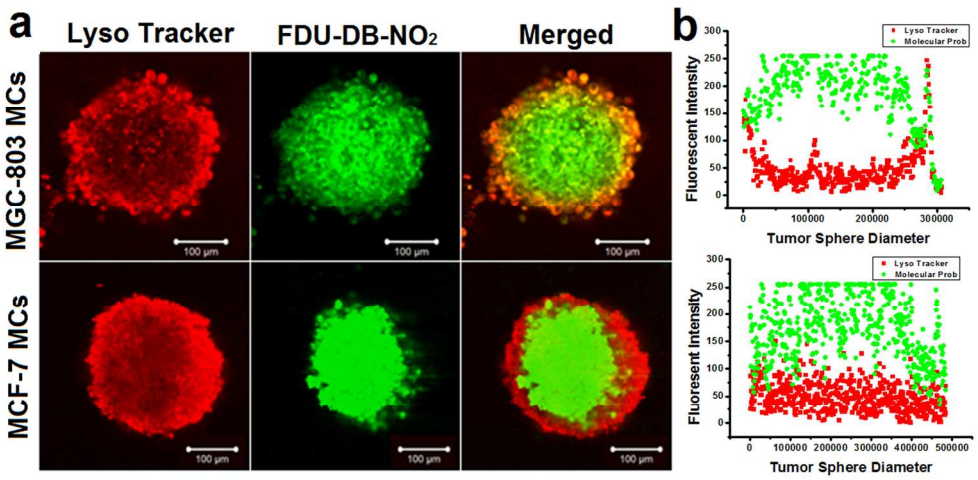

Figure 3

170x84mm (300 x 300 DPI)

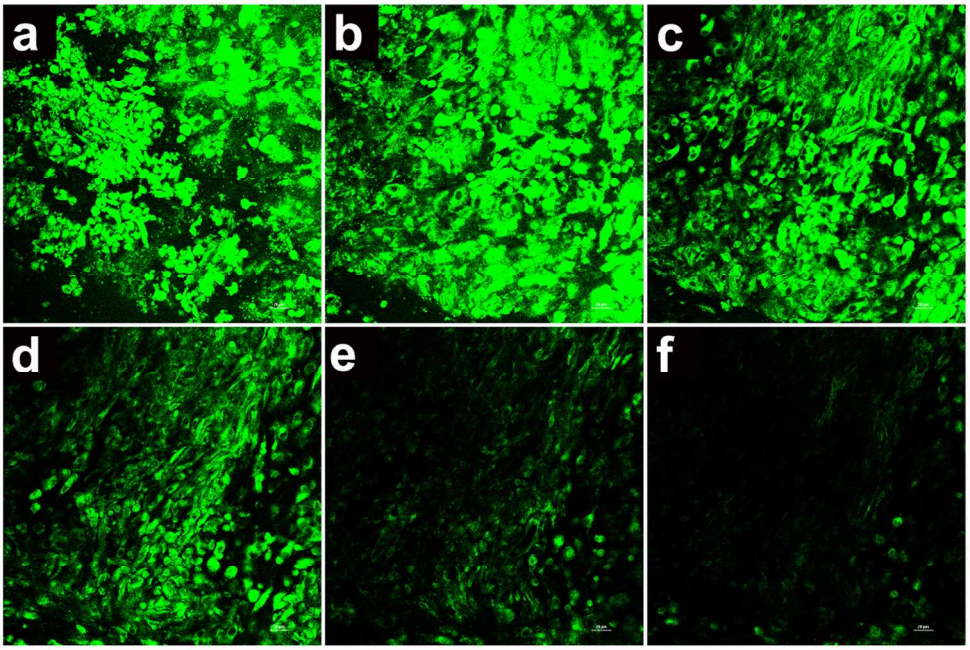

Figure 4

109x73mm (300 x 300 DPI)

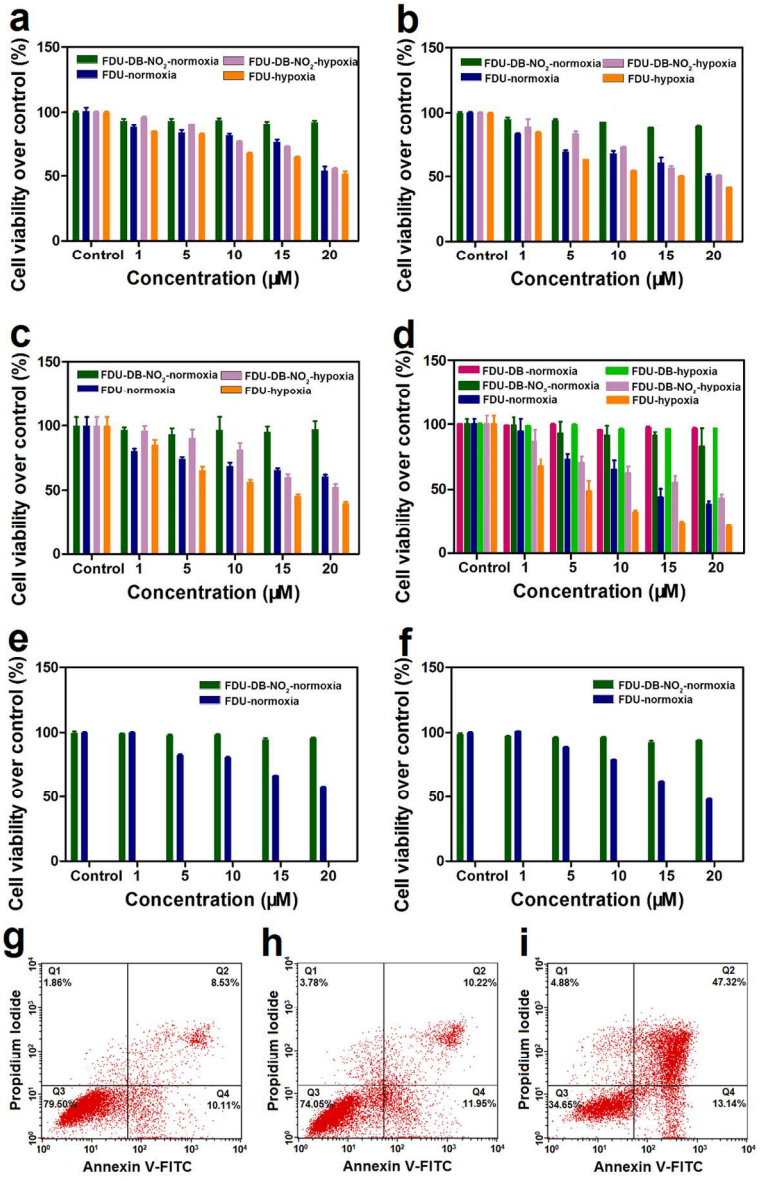

Figure 5

127x191mm (300 x 300 DPI)

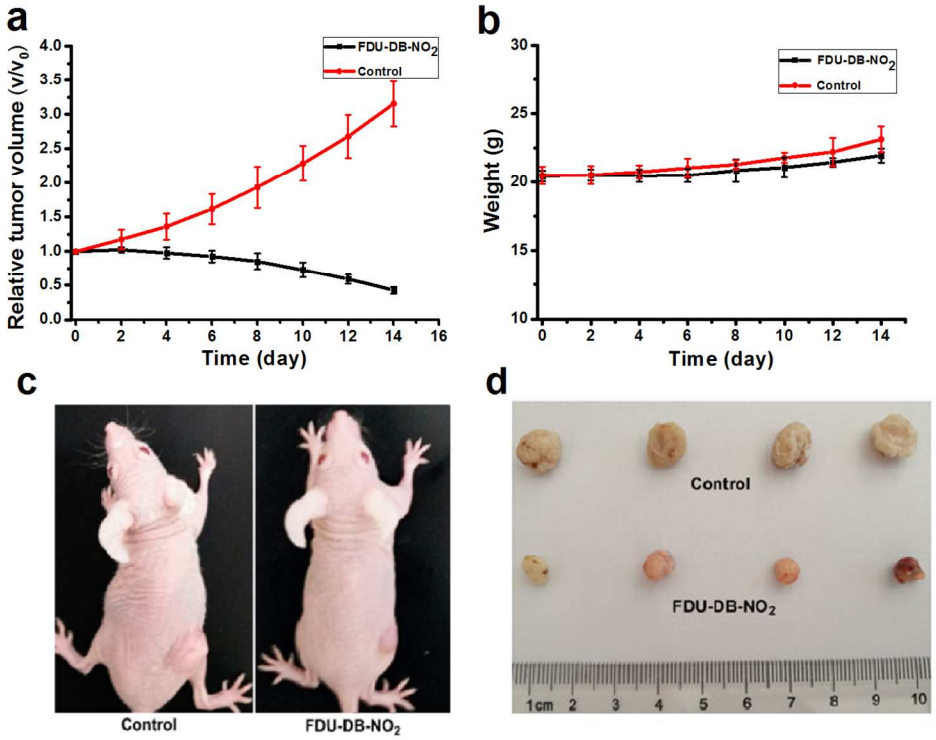

Figure 6

126x98mm (300 x 300 DPI)